Towards a Mechanistic Understanding of One of the Rainiest Spots on Earth

John F. Mejía[1], Johanna Yepes[1,2], Juan J. Henao[3], Germán Poveda[2], Manuel D. Zuluaga[2], David J. Raymond[4,5], and Željka Fuchs-Stone[4,5]

1. Division of Atmospheric Sciences, Desert Research Institute
2. Department of Geosciences and Environment, Universidad Nacional de Colombia, Medellín, Colombia
3. GIGA, Escuela Ambiental, Facultad de Ingeniería, Universidad de Antioquia, Medellín, Colombia
4. Climate and Water Consortium, New Mexico Tech, Socorro, NM, USA
5. Physics Department, New Mexico Tech, Socorro, NM, USA

Mejía: https://orcid.org/0000-0001-6727-5541
Yepes: https://orcid.org/0000-0002-2177-2777
Henao: https://orcid.org/0000-0002-1141-7683
Poveda: https://orcid.org/0000-0002-7907-6360
Zuluaga: https://orcid.org/0000-0002-7184-9752
Raymond: https://orcid.org/0000-0002-9877-6450
Fuchs-Stone: https://orcid.org/0000-0001-5890-4211

Submitted to Journal of Geophysical Research: Atmospheres

Abstract

According to TRMM and GPM satellite precipitation composites, a broad maritime area over the far eastern Tropical Pacific and western Colombia houses one of the rainiest spots on Earth. This study aims to present a suite of mechanistic drivers that help create such a world-record breaking rainy spot. Previous research has shown that this oceanic and nearly-continental precipitation maximum has a strong early morning precipitation peak and development of a high density of mesoscale convective systems. We examined new and unique observational evidence highlighting the role of both dynamical and thermodynamical drivers in the activation and duration of organized convection. Results show the existence of a rather large combination of mechanisms, including: (1) dynamics of the Choco (ChocoJet) and Caribbean Low-Level Jets along their confluence zone, including the Panama semi-permanent low; (2) land breeze favors ChocoJet deceleration offshore, enhancing the nighttime and early morning low-level convergence; (3) vertical wind shear and tilting of vertical wind shear into vorticity lines that interact with convective outflows; (4) action of mid-level gravity waves, which support the strong diurnal variability; (5) mesoscale convective vortices related to subsidence in the stratiform region in long lasting MCSs reinforcing (3); and (6) the likely role of land surface-atmosphere interactions and the rainforest over western Colombia. This study emphasizes the multi-scale environmental processes associated with the formation of one of the rainiest spots on Earth and showcases new observations gathered during the Organization of Tropical East Pacific Convection (OTREC; August-September, 2019) which support the outlined mechanisms.

1 Introduction

The latest generation of satellite precipitation products (Global Precipitation Measurement, hereafter GPM; Huffman et al., 2018) show that rainiest spots on Earth is located over the far Eastern Pacific (hereafter refer to as far EPAC) region, offshore from the Colombian coast with 25.42 mm day^{-1} (9278 mm $year^{-1}$; averaged over 2000-2019; Figure 1). Previous studies have also highlighted this tropical area as one of the rainiest places on Earth (Poveda and Mesa, 2000; Sakamoto et al., 2011; Vallejo-Bernal et al., 2020). Snow (1976) and Poveda and Mesa (2000) reported rain gauge measurements showing maximum values exceeding our GPM record (e.g., Lloró with a historical record of 12,541 mm $year^{-1}$); these rain gauges were located between the outlined GPM maximum and the Western Andes foothills. We acknowledge that GPM products suffer from calibration and scale issues (0.1° × 0.1° grid size; Tang et al., 2020) and that there are sites like Lloró or other places on Earth showing long-term rain gauge records exceeding this record-breaking GPM-based estimate. Regardless of the inherited uncertainties of the remote sensing precipitation products (Vallejo-Bernal et al., 2020), the region offshore the Colombian Pacific coast shows a striking, broad, coherent area of precipitation maximum.

This precipitation hotspot sustains the Chocó rainforest, regarded as one of the most biologically diverse areas in the world (Grau and Aide, 2008), and modulates the hydroclimate of Central America and NW South America (Poveda, 2004; Rueda and Poveda, 2006; Poveda et al., 2006; Poveda et al., 2014; Durán-Quesada et al., 2012; Ma et al., 2018; Loaiza et al., 2020). The EPAC is genesis region of Tropical Storms/Tropical

Cyclones (Serra et al., 2010) and other extreme convection events that affect NW South America, Central America and even Western Mexico and SW US (Mejía et al., 2016), which can have long lasting consequences in the economy and security of the regions (Christoplos et al., 2010; Murakami et al., 2013). Results from modeling sensitivity experiments using a regional climate model showed that Mesoscale Convective Systems (MCSs) in the far EPAC (Velasco and Frisch, 1987; Mejía and Poveda, 2005; Zuluaga and Houze, 2015; Jaramillo et al., 2017) can be a significant contributing factor adding variance to Tropical Easterly Waves (TEW) affecting the far EPAC cyclogenesis core (Rydbeck et al., 2017). Measuring and understanding the local drivers that favor convection and the upscale effects as the environment reacts to such precipitation and heating disturbances (Huaman and Takahashi, 2016; Schneider et al., 1997) can help us to understand the dynamical and thermodynamical processes involved in this rainy region, and to address whether the parameterized models or increasing model resolution in IPCC-WRCP Assessment Report model experiments are improving model fidelity and reducing model uncertainty (Kharin eta al., 2007; Copola et al., 2014; Baranowski et al., 2019; Na et al., 2020), thus leading to better prediction and projections of mean and extreme events.

Two main regional low-level flow features have been documented to partly modulate the far EPAC precipitation regimes and spatial patterns: the Caribbean Low-level Jet (CLLJ) and Choco LLJ (hereafter referred to as ChocoJet; Poveda and Mesa, 1999; 2000; Yepes et al., 2019; Yepes et al., 2020). CLLJ is an important component of Intra-Americas Sea circulation patterns (Poveda and Mesa, 1999; Amador, 2008) and is related to the enhanced easterly low-level flow over the central Caribbean. The variability of the

easterly trade winds and the CLLJ modulate the intensity of gap flows over Central America and into the Pacific coast, namely the Tehuantepec Jet, Papagayo Jet and Panamá Isthmus Jet. On the other hand, ChocoJet is related to the southwesterly component of the trans-Equatorial trade winds located over the far EPAC and can extent upstream as far south as the Chilean coast (Sakamoto et al., 2011). Both ChocoJet and CLLJ are the main components of the mean and transient states of the ITCZ in the EPAC region and play a significant role in providing moisture to the surrounding land regions (Durán-Quesada et al., 2012). The confluence of ChocoJet and CLLJ over the far EPAC and their interaction with the Andes mountains have been linked to convection activation that results in the outlined precipitation hotspot (Arnett and Steadman, 1970; Snow, 1976; Poveda and Mesa, 2000; Mapes et al., 2003; Sakamoto et al., 2011; Poveda et al., 2014; King et al., 2017; Jaramillo et al., 2017; Yepes et al., 2019; Espinoza et al., 2020; Poveda et al., 2020), and provide the favorable conditions for the increased occurrence of MCSs when both CLLJ and ChocoJet converge over the region (Zuluaga and Houze, 2015).

A substantial proportion of the precipitation in the far EPAC falls from MCSs (Velasco and Fritsch, 1987; Zuluaga and Houze, 2015, Jaramillo et al., 2017). Jaramillo et al. (2017) showed that MCSs contribute to 57% of total rainfall over the region (60% based on general tropical estimates; Roca et al., 2014). Over the far EPAC, Jaramillo et al. (2017; Figure 4) showed that offshore MCSs features tend to develop early in the morning, whereas non-MCSs convection tends to form over the costal lowlands and foothills of the Western Andes but predominantly during the afternoon. Mejía and Poveda (2005) used reanalysis products to estimate convective indices around MCSs identified using the Tropical Rainfall Measuring Mission (TRMM) measurements. They

found that the environments related to MCSs in this region include enhanced CAPE, suppressed CIN, and moderate vertical shear. The formation of early morning MCSs has been linked to the propagation of the cool phase of a gravity wave (GW) that emanates from the Andes during the afternoon and moves offshore (Mapes et al., 2003; Warner et al., 2003; Biasutti et al., 2012; Jaramillo et al., 2017; Yepes et al., 2019, 2020), with its cold phase helping to reduce the inhibition built by the layer of warmer and drier easterly trade winds flowing over the Andes and moving over the relatively low-level cooler and moist westerly ChocoJet (Yepes et al., 2020). However, the forcing mechanisms for the offshore and early morning maximum can also be related to the land breeze circulation and mechanically forced gravity waves (Coppin and Bellon, 2019; Wang and Sobel, 2017); or some form of gravity waves induced by afternoon convection farther inland to the east (Ruppert and Zhang, 2019). For tropical MCSs, low-to-mid tropospheric wind shear is believed to modulate storm severity (Liu et al., 2020) and lifetime (Weisman and Rotunno, 2004; Hagos et al., 2013; Chen et al., 2015). Low-level shear can favor the generation of new cells by interacting with the storm's cool pool and surface and boundary layer fluxes, whereas mid-level shear tends to interact with the warm core mesovortices --induced by subsidence in the stratiform region vertical momentum and vorticity advection (Zuluaga and Houze, 2015; Rydbeck et al., 2017)-- and modulate the mid-level moisture convergence and convection strength and organization (Velasco and Fritsch, 1987; Chong and Bousquet, 1999; Houze, 2004). Although some far EPAC regional modeling efforts have been performed to examine some of the processes outlined above, few *in situ* observations are available to study the variations of the basic

states conducive to this exceptional generation of nocturnal and early morning MCSs and precipitation.

Much of the work over EPAC is related to convection and mesoscale structures (Raymond et al., 2004), but little has been developed to understand how regional circulation basic states and their day-to-day variations modulate the dynamics and thermodynamics of precipitation in the region. The formation and characteristics of convective organization and precipitation, as well as its relationship to the CLLJ and ChocoJet, have strongly relied on remote sensing and reanalysis data or very short modelling experiments (Mapes et al., 2003; Warner et al., 2003). Few studies focused on testing the fidelity of these data in representing the tropospheric circulation features of the far EPAC (Colombian Pacific). Two elements make this needed research difficult to pursue: first, the land/water distribution makes observational networks (surface and upper-air) far from ideal, and secondly, the sparse operational network is intermittent and targeted to satisfy basic operational tasks.

To fill some of the outlined scientific gaps, the Chocó Jet Experiment (ChocoJEX) was developed during 2016 to observe and model the dynamics and thermodynamics of ChocoJet (Yepes et al. 2019, 2020). ChocoJEX helped to confirm the model-based GW hypothesis as a mechanism favoring the early morning offshore convective hotspot. During Aug-Sept 2019, a field campaign called Organization of Tropical East Pacific Convection (OTREC; Fuchs-Stone et al., 2020) was developed over the East Pacific and extreme SW Caribbean to understand basic process that govern convection in the region. Based on OTREC dropsonde measurements Fuchs-Stone et al. (2020) showed that the far EPAC exhibits deeper convection and different

thermodynamic characteristics than those at corresponding latitudes in the EPAC and Western Caribbean. For example, they found that relative to the EPAC and Western Caribbean region, the saturation fraction (a proxy for precipitation amount) over the far EPAC is less sensitive to low- to mid-tropospheric moist convective instability, which further justifies seeking for other environmental mechanisms that help support the deep convection in the area. It is worth noticing that this region exhibits the highest omega values at 300 and 200 hPa worldwide, according to diverse reanalysis (Figure A-3).

Within OTREC, a radiosonde site strategically-located in Nuquí, along the shoreline of the Colombian Pacific (5.7096° N, 77.2667° W; hereafter OTREC-Nuquí), was established as a systematic field campaign effort to fill a surface and upper-air observational gap over the far eastern Pacific (EPAC) and western Colombia, and to support and complement the OTREC field campaign program. OTREC-Nuquí enabled us to measure the environmental conditions favoring and controlling the GPM precipitation record value, and its day-to-day and diurnal variability.

The objective of this study is to present OTREC-Nuquí measurements and discuss the day-to-day and diurnal circulation and thermodynamics mechanisms that favor the existence of one of the rainiest places on Earth. First, we describe the novel OTREC-Nuquí observations consisting of systematic and frequent radiosonde observations and other OTREC observation platforms utilized here, including the NCAR Gulfstream-V aircraft dropsonde data. Satellite and reanalysis datasets are also implemented and examined by compositing the atmospheric environments to categorize days with significant MCSs development (related to high precipitation days). Then, we examine the mean flow conditions and describe the dynamical and thermodynamical

characteristics related to MCSs development (or lack thereof), as well as the structure and shape of the GW phenomenon. We also present other surface and upper-level features driven by the complex topography, by the tropical rainforest and the coastal shapes in the area. The sections are organized as follows: Section 2 presents the OTREC-Nuquí data and other ancillary datasets, including the methods used to categorize MCS events; Section 3 presents the results, followed by a summary and concluding remarks in Section 4.

2 Data and Methodology

2.1 OTREC Nuquí Soundings

OTREC-Nuquí site was established as a unique and systematic observational effort to fill surface and upper-air observational gaps over the far eastern Pacific and western Colombia, and to support and complement the NSF-OTREC field campaign program (Voemel et al. 2019; Fuchs-Stone et al., 2020). Nuquí is a small town located at the shoreline of the Pacific Coast of Colombia (77.26°W, 5.71°N) near one of the rainiest spots on Earth (Figure 1a). Field campaign details, quality assurance/quality control procedures and other details are described in Mejía and Poveda (2020). Soundings were performed using a Vaisala DigiCORA MW41 Sounding System and Vaisala RS41-SGP radiosondes. Protocols were developed to transmit the observations in real-time for field campaign support and assimilation by global forecasting systems. The OTREC-Nuquí site consisted in twice a day (00 and 12 UTC) upper-air radiosondes launched from 5th August to 25th September, 2019, with two additional launches (06 and 18 UTC) on the days of the 22 research flights of the NSF/NCAR Gulfstream-V (G-V). Nine of these research flights took place off the Pacific coast of Colombia. Nuquí soundings provided

in-situ observations to characterize the circulation and thermodynamics convection indices associated with the observed convective activity in the region. Unless stated explicitly, composites use all the soundings available, but daily indices only average the 00 and 12 UTC soundings.

Additionally, we show an analysis of the August 11, 2019 research flights to examine the mesoscale features taking place during one MCS event off the Pacific coast of Colombia. Details of the 3DVAR analysis approach and early OTREC results on the vertical characteristics of convection in the region are shown in Fuchs-Stone et al. (2020). The data set for dropsondes used in the 3DVAR analysis is NCAR/EOL AVAPS Dropsonde Quality Controlled Data Version 1.0 (Voemel, 2019).

2.2 Reanalysis ERA5

This study uses regional circulation composites based on the European Center for Medium-Range Weather Forecasts ERA5 reanalysis at $0.25^{o} \times 0.25^{o}$ grid size and hourly time increments (C3S, 2017; Hersbach et al., 2020). OTREC-Nuquí data and other OTREC upper-air sounding sites in Costa Rica were transmitted to the Global Telecommunication System (GTS) systems and are presumed to be assimilated by the forecasting agencies. UCAR/NCAR - Earth Observing Laboratory registered the sites and provided the connection platform for promptly delivery of the observations to the GTS. By the time this study was developed there were no records of the success in the transmission and assimilation of the data. It is likely that a few (3 out of 141) delayed soundings were not assimilated (see Mejía and Poveda, 2020 for details). For completeness, we also use independent measurements (not made available to the GTS) from five surface stations from the meteorological network managed by the Red de

Medición de Parámetros Oceanográficos y de Meteorología Marina/Dirección General Marítima (hereafter referred to as DIMAR). DIMAR observations were quality assured/quality controlled by visual inspection and basic diurnal and composite distribution assessment. Although these surface station sites proved to be very useful, we highlight some siting constrains and data quality issues that limited the insight they provided.

2.3 GPM Satellite

Precipitation fields in this paper use the NASA Global Precipitation Measurement-interpolated and intercalibrated merge data (GPM-IMERG V06B; Huffman et al. 2018; hereafter GPM) for 2000-2019. These GPM products combine satellite microwave precipitation estimates, together with microwave-calibrated infrared (IR) satellite estimates, into final values calibrated against precipitation gauges. Products are created at half-hourly time increments and 0.1° × 0.1° as spatial grid size, which enable adequate the detailed characterization of the diurnal cycle of precipitation for this study (Tan et al. 2019). The GPM data were also used to examine precipitation spatio-temporal patterns, from diurnal to day-to-day scales during OTREC campaign (August-September, 2019).

2.4 MCSs and Wet and Dry Days

In this study we used the GPM data and adapted Liu et al. (2019) methods to identify MCSs. Liu et al. (2019) used 3-hourly TRMM-3B42V7 data available at 0.25° grid size to classify MCS as coherent spatial clusters of precipitation rates exceeding 25mm/day and larger than 2000 km^2 in size. Here, we use the same threshold and size criteria but also constrain the cluster in time to benefit from the half-hourly data. A precipitation cluster is part of the same MCS if there is at least 25% area overlap between

consecutive time increments. We tested the sensitivity of the precipitation threshold and the overlap area criteria and found that the approach is robust in uniquely identifying MCS events. Herein, we use the days with MCSs occurring over the Colombian Pacific region (3.5° N – 7° N, 82° W – 76° W) lasting more than 6 h to define days with enhanced convection activity (hereafter Wet days; see MCS trajectories in Figure A-1); days with less organized, scattered showers are defined as relatively drier days (hereafter Dry days). Based on these criteria, a total of 19 (31) days are considered Wet (Dry) days.

This study does not address the relationship of MCSs to TEW or any other source of synoptic variability in the area. An aspect adding robustness to the discriminatory power of the environment of our Wet and Dry index is that at this time of the year the daily precipitation in the study region does not correlate well to daily precipitation over the Western Caribbean (Pearson correlation coefficient of 0.16; 9° N – 13° N, 83.5° W – 80° W), where sub-seasonal burst and breaks appear more apparent and more strictly linked to TEW passages (or lack thereof) and other large-scale conditions adding lower-frequency variability, such as the phase of the Madden-Julian Oscillation (Poveda et al., 2005). Therefore, it is fair to suggest that departures of the environmental conditions related to Wet or Dry days favor or suppress MCS development, which in turn lead to the copious precipitation record within the westward moving maritime precipitation signal.

MCS characteristics, including duration and size, depend on their definition. For example, it is likely that more or different days could be considered as MCS days if they were characterized by their cloud-top temperature or mid-tropospheric vorticity signatures. For all composite estimates in this study we tested their statistical robustness

by bootstrapping --with replacement—Wet and Dry days. Unless otherwise described, most composite results are robust and independent of MCS definition and precipitation threshold.

3 Results

3.1 Precipitation During OTREC

Figure 1a shows that the eastern end of the ITCZ over the EPAC, just off the Colombian coast, houses a coherent precipitation maximum with 25.4 mm day^{-1} (77.6º W, 3.9º N), with the rainy season peaking between August-October (not shown; Mejía et al., 1999; Martinez et al., 2019). This seasonal peak coincides with the northernmost extent of the ITCZ over the EPAC and the west Atlantic regions (Martinez et al., 2019). Figure 1c, d show the climatological conditions for August-September precipitation emphasizing the copious amounts of precipitation that fall over the far EPAC, and the precipitation and anomaly patterns during the OTREC campaign (August-September, 2019), respectively. During OTREC, precipitation anomalies show a meridional dry-wet pattern suggesting that the ITCZ was anomalously shifted northward, a condition that has been linked to a relatively weak CLLJ (Hidalgo et al., 2015). TEW frequency and intensity and MJO-like modes can also modulate the ITCZ location and precipitation over the EPAC (García-Martínez et al., 2020). For example, over the far EPAC the active phase of the MJO tends to shift the region of active convection east and northward (Molinari and Vollaro, 2000), and to intensify the amplitude of the diurnal cycle of rainfall over the Andes of Colombia (Poveda et al., 2005). Two MJO active phases were reported over the Western Hemisphere during OTREC, a mild and short incursion during mid-August, and a longer and stronger incursion during the second half of September

(using the MJO monitoring index from the Australian Government, Bureau of Meteorology). Although other subseasonal to seasonal and circulation patterns could have helped redistribute the regional precipitation, this study assumes that the outlined precipitation anomalies do not preclude examining the day-to-day mechanisms (sub-synoptic temporal scales) that took place.

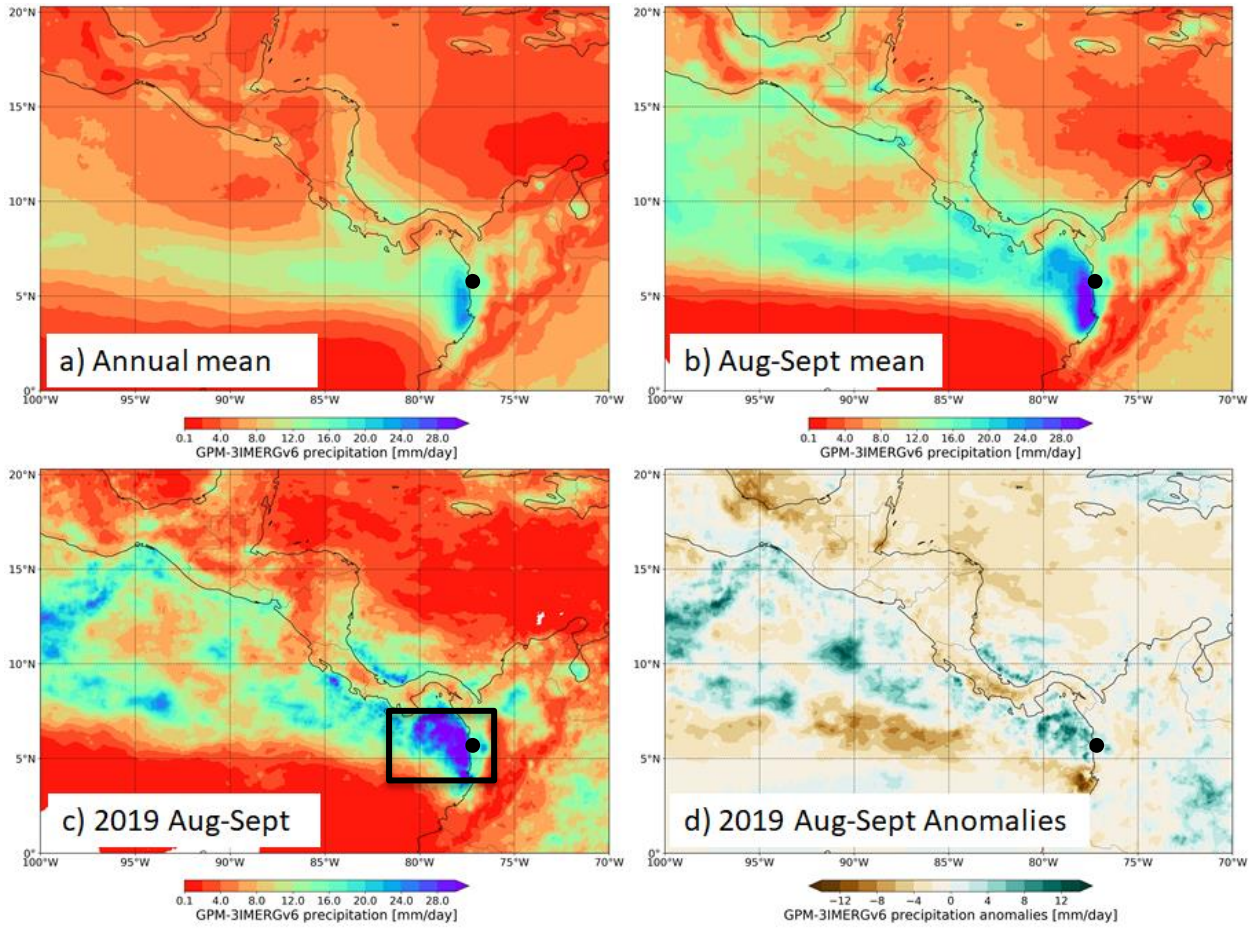

Figure 1 GPM-IMERG precipitation over EPAC for: a) Long-term (2000-2019) annual mean, b) long-term August-September mean, c) August-September, 2019 and d) 2019 August-September anomalies. Nuquí location is indicated by the black dot. Precipitation averages were performed in the box (3.5° N - 7° N, 82° W – 76.5° W) indicated in (a).

Figure 2a shows a longitudinal transect of the diurnal cycle of precipitation during OTREC, averaged between 3.5° N - 7° N. Of note is the westward propagation of convection starting late afternoon over the western slopes of the Andes, moving

317 westward over the coast by 03-04 UTC (22 – 23 Local Time; -5 GMT) and extending
318 several hundreds of kilometers into the ocean. The outlined westward propagation seems
319 to start at 07-08 UTC (02-03 LT). A striking feature in this westward propagation of
320 precipitation is the burst of intense and relatively narrow embedded precipitation band
321 (50-100km) just offshore (78° N and the coast), reaching a maximum in precipitation at
322 around 11-12 UTC (05-06 LT). This pronounced burst is collocated with the record-
323 breaking precipitation hotspot (Figure 1) and coincides with the preferred timing of the
324 upscale growth of convection into MCSs shown in Jaramillo et al. (2017); this region has
325 the highest frequency of cloud clusters on Earth (Hennon et al., 2013), and contains the
326 largest values of vertical velocity (omega) at 300 hPa in the world (Figure A-3).
327 Figure 2b-c show composites of the diurnal cycle discriminating Wet and Dry
328 days. Not surprisingly, Colombian coast Wet days have a more intense and apparent
329 westward propagation characteristic. The strong maritime diurnal cycle of precipitation
330 with such long-range has been documented in several locations around the world (Yang
331 and Slingo, 2001; Mapes et al., 2003; Huang et al., 2018; Yokoi et al., 2019; Yulihastin et
332 al., 2020). For example, the west coast of Sumatra shows similar precipitation diurnal
333 characteristics, including the westward propagation of long-lasting convective clusters
334 mainly driven by low-level vertical shear (Yokoi et al., 2019). Over the Colombian
335 Pacific, it has been linked with the propagation of gravity waves that emanate from the
336 Andes (Mapes et al. 2003; Jaramillo et al., 2017; Yepes et al., 2019, Yepes et al., 2020).
337 In the following sections, we reinforce these connections and postulate other plausible
338 mechanisms revealed by the OTREC-Nuquí measurements.

Figure 3 shows the longitudinal evolution of precipitation over the 3.5° N - 7° N belt highlighting the westward moving characteristics of convection clusters in the form of MCSs, with a significant 2- to 5-day spectral signal (not shown). Note that some westward moving MCSs over the far EPAC (represented by the continuous long-lasting burst of precipitation) are related to westward moving precipitation signatures over the Andes, while others appear to develop without preexisting signatures. It is likely, however, that not all westward moving synoptic disturbances are convectively coupled over the Andes. Alternatively, it is possible that some of the day-to-day variability is locally generated over the far EPAC (Rydbeck et al., 2017). The relationship of precipitative systems to convectively coupled waves will be developed as a separate study.

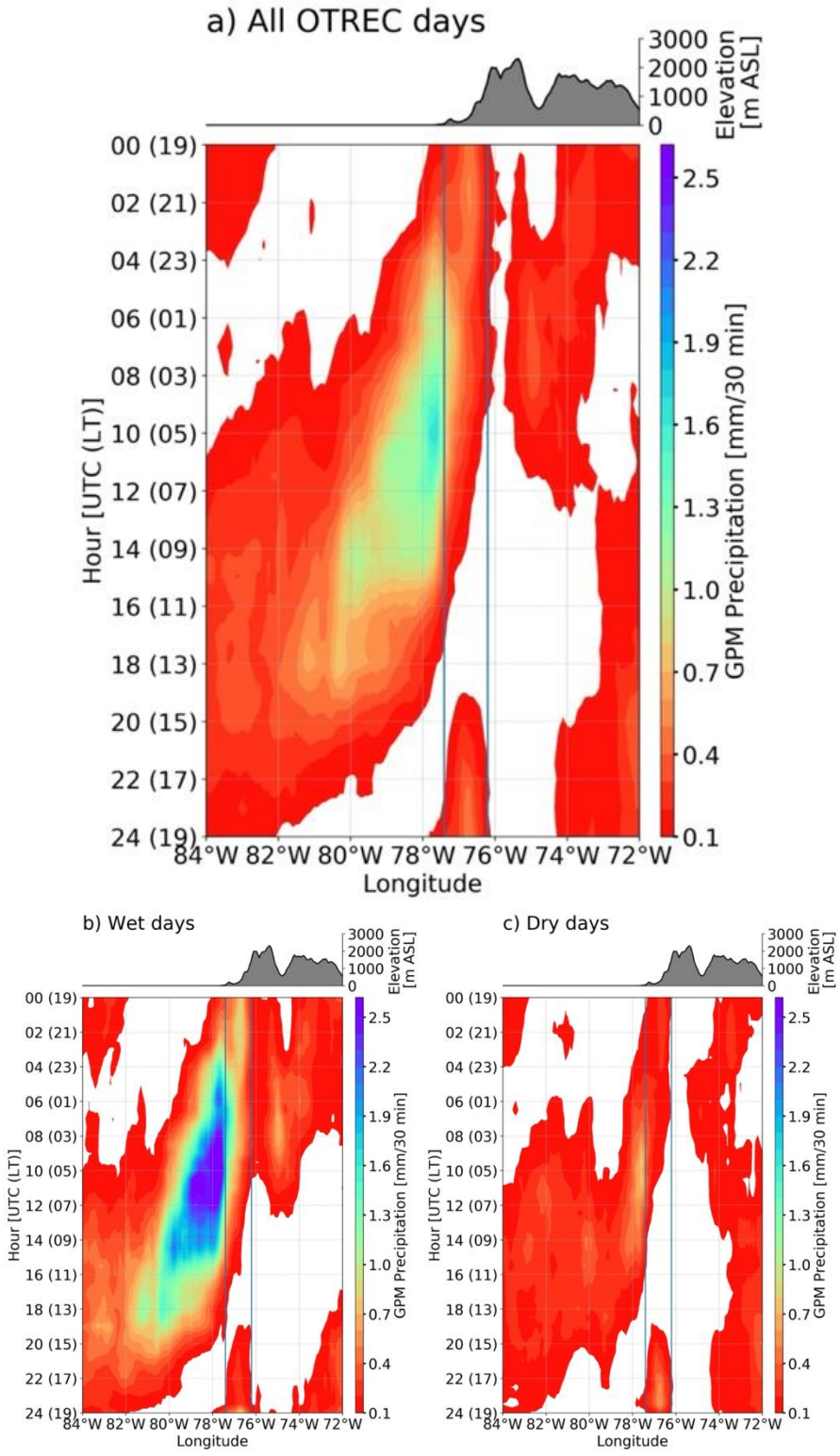

Figure 2 Longitudinal transect of the diurnal cycle based on GPM-IMERG precipitation (mm/30 min) averaged between 3.5° N - 7° N during OTREC (Aug-Sept, 2019). Blue lines indicate the longitudinal

location of Nuquí over the Colombian Pacific coast (77.4° W) and the western range rim over the Andes (76.2° W).

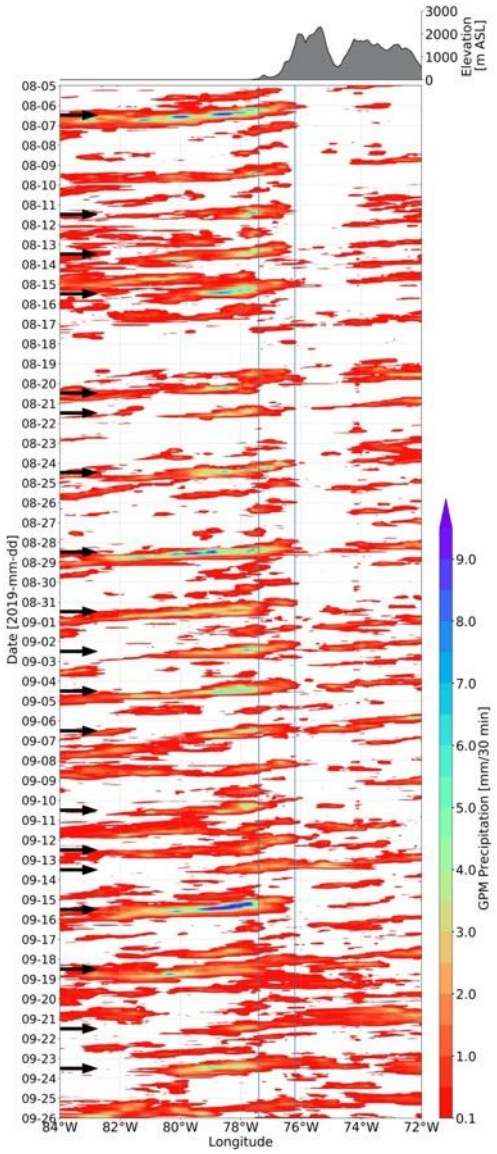

Figure 3 Longitudinal Hovmöller diagram of GPM-IMERG precipitation using 30 min time increments averaged between 3.4° N - 7° N during OTREC (Aug-Sept, 2019). Blue lines indicate the longitudinal location of Nuquí over the Colombian Pacific coast (77.4° W) and the western range rim of the Andes (76° W). Arrows indicate MCS development days (Wet days).

3.2 On the Observed Circulation

3.2.1 Nuquí Vertical Composites

The ChocoJet is a prominent climatic feature over the Far Eastern Pacific (EPAC) and one of the dynamic forces that supports the rainiest place on Earth (Poveda and Mesa

1999, 2000) during September-October-November. The presence of ChocoJet over the Colombian Pacific has been linked with moisture transport from cold waters of the tropical EPAC into the Andes mountains over NW South America (Rueda and Poveda, 2006; Poveda et al., 2006, 2014, 2020; Espinoza et al., 2020), which by orographic lifting along with relatively drier easterlies at mid-levels help produce unstable conditions further reinforcing the precipitation record. Recently, the ChocoJEX experiment measured the ChocoJet for the first time and shed some light on its role in precipitation generation (Yepes et al., 2019). Now, OTREC-Nuquí offers longer and more systematic measurements of the ChocoJet and how its variability is related to convection and its organization into MCSs.

Figure 4a-c show the wind, specific humidity and moisture flux profiles composited by Wet and Dry days, respectively; Figure 4d-e show corresponding Wet minus Dry differences and their statistical significance. In general, Nuquí wind profiles show a pronounced southwesterly "nose-shaped" characteristic of a low-level jet flow with maximum at 500-750 m (950-925 hPa) and confined below 2000 m. Wet and Dry wind composites highlight that ChocoJet is significantly enhanced and more southwesterly during Wet days. Low-level specific humidity also increases during Wet days resulting in an enhancement of zonal moisture flux convergence over the western slopes of the Andes. When ChocoJet hits the western slopes of the Andes, orographic lifting occurs and creates a large gradient of precipitation with a local maximum starting during the afternoon (15 LT) over the western foothills and a precipitation shadow to the east (Figure 2). Therefore, MCS occurrences appear to be strongly discriminated by ChocoJet intensity, which broadly agrees with findings based on reanalysis products. For example,

388 at the storm scale, Zuluaga and Houze (2015) found that deeper and more organized
389 storms systems were related to an 850 hPa westerly wind anomaly and its interaction with
390 the Andes. Furthermore, at seasonal-to-interannual scales, a stronger than normal
391 ChocoJet has been related to anomalously wet seasonal patterns over Colombia (Poveda,
392 2004; Poveda et al., 2006; Arias et al., 2015; Bedoya-Soto et al., 2019).

393 At around 2000 m ASL, the OTREC Nuquí wind profiles change from southwesterly
394 to mostly easterly-southeasterly (Figure 4). This rather sharp sign change in the zonal
395 component coincides with the mean height of the Andes western range (see elevation
396 inset in Figure 2), and with the location of the mid-level easterly atmospheric jet crossing
397 over the Andes from NW South America into the Pacific Ocean (Poveda and Mesa,
398 1999). Throughout OTREC field campaign, the easterly trade winds prevail over the
399 Andes. Above the Andes and up to 4000 m, Wet days are related to a significant
400 enhancement of the southeasterly wind component linked to a layer of enhanced specific
401 humidity (Figure 4b, e). These results suggest that convection organization is also linked
402 to enhanced mid-level moisture flux convergence. These day-to-day transient scale
403 results support the role of the northern Amazon climatological airflow pathways as
404 source of moisture convergence over Western Colombia suggested by Sakamoto et al.
405 (2011), Poveda et al. (2014) and Hoyos et al. (2018). Note that by construction the local
406 enhancement of convection organization and precipitation could be partly responsible of
407 the outlined moistening of the atmosphere (Figure 4e). A detailed moisture budget
408 analysis can help elucidate the relative role of surface and low- to mid-level moisture
409 sources in convection organization.

a) b) c)

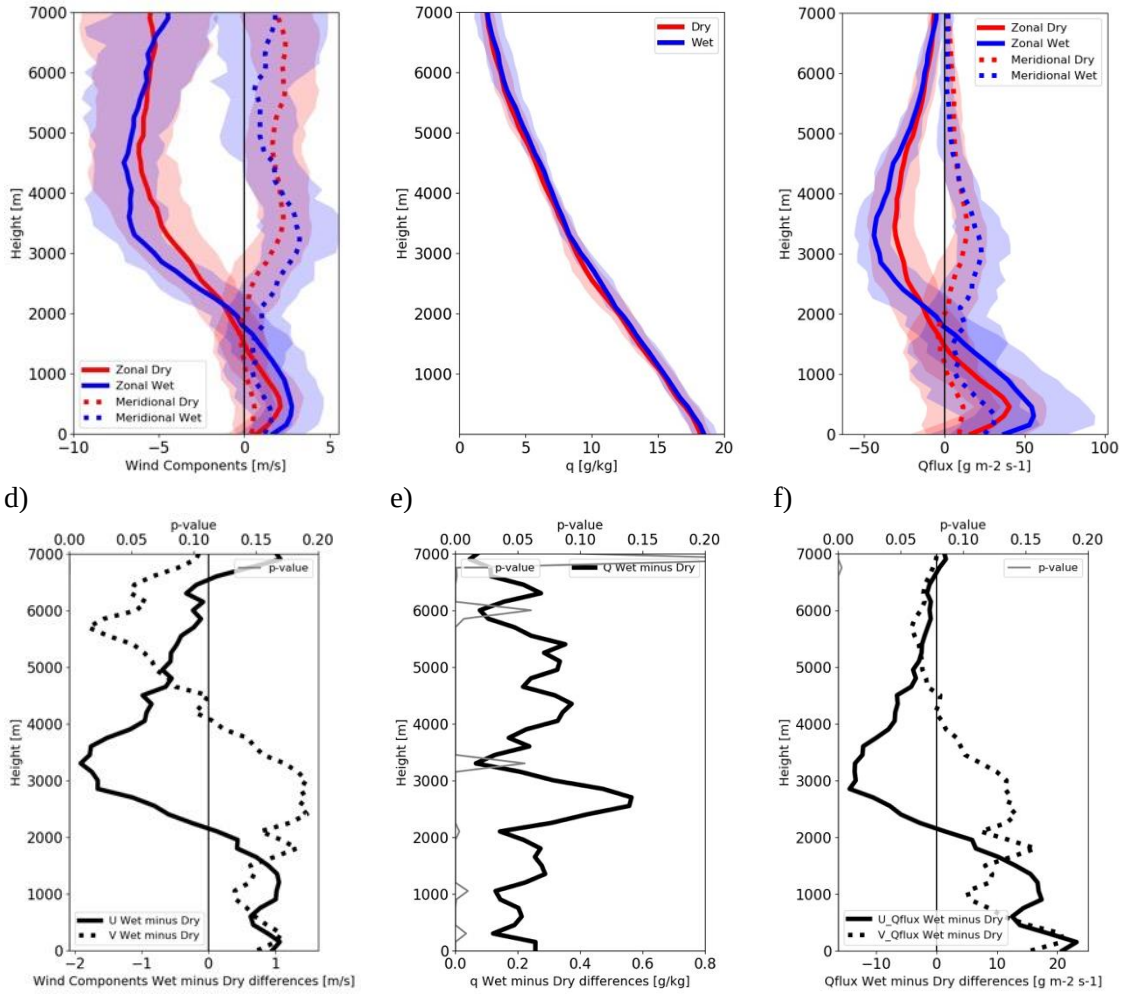

410 Figure 4 OTREC-Nuquí (August-September, 2019) wind vertical composites during convectively active
411 (Wet) and non-convective (Dry) days (assuming 00-23UTC days) for (a) zonal (U) and meridional (V)
412 median wind, (b) specific humidity, and (c) moisture flux. Shaded areas show the interquartile range of
413 each composite sample. (d-f) show the respective Wet minus Dry differences and one-sided p-values
414 evaluating the significance of the sample independence using the Student's t-test.

415 To identify the diurnal relationships of the circulation and precipitation, Figure 5
416 shows the zonal Wet and Dry wind profiles further composited by time of the day, 00
417 UTC (19 LT; late afternoon) and 12 UTC (07 LT; early morning). In general, results
418 show discernable changes in amplitude of local circulation according to the convection
419 regime. Assuming that day-to-day variation of ChocoJet is derived from regional- to

large-scale drivers, then we list the possible drivers of such differences in the local circulation:

1. *Land and sea breezes*: Not surprisingly for this coastal site, and regardless of the convective regime, results show that the sea breeze reinforces ChocoJet during the afternoon, while the land breeze decelerates the flow early in the morning. Even though the prevailing near-surface wind is westerly-southwesterly, the Nuquí soundings show that there are days with an early morning offshore wind component in the surface winds. The occurrence of an offshore flow seems to be more consistent during Dry days, as showed by the weaker westerly flow and more concentrated distribution of offshore wind component. Locally, this offshore flow can be related to a combination of drainage flow due to high elevations (a few hundred meters height) near the coast and the inertial thermal contrast. It is likely that drier and less cloudy environments allow more inland cooling at night, facilitating the occurrence of the rather shallow offshore wind.
2. *Diurnal cycle amplitude:* A striking feature in Figure 5 is the contrasting differences between AM and PM composite zonal wind medians during Wet and Dry days for the low-level winds. Wet day composites show that ChocoJet is much stronger during the afternoon and weaker during the morning, whereas Dry composites show relatively smaller diurnal cycle differences. Surface flow to the east of Nuquí (inland direction) implies that Wet days are related to a significantly stronger ChocoJet, which might increase the low-level moisture convergence as the flow approaches the Andes. The nighttime and early morning precipitation burst is related to a stronger deceleration of ChocoJet, likely due to the land-breeze

enhancing the low-level moisture convergence offshore of the Nuquí location. The offshore scale of the precipitation burst (Figure 2) further supports this idea as land breeze influence scales typically range ~50-100 km (Drobinski and Dubos 2009).

3. *Sequence of events:* Vertical profiles of wind composites provide supporting evidence of diurnal cycle of circulation and its relationship to the propagating precipitation signature suggested in FiguresFigure 2 and Figure 3. During the afternoon, the enhanced ChocoJet triggers storms over the foothills and western plains. By nighttime, convection organizes and propagates towards the coast, with related cold pools and convective outflows supporting the enhanced thermal contrast that help deaccelerate ChocoJet (Mejía et al., 2016). Of note is that Wet AM composites (Figure 5) show a deeper ChocoJet deacceleration contrasting the shallower Dry AM easterly wind profile described above. By early morning, the Wet AM wind composites suggest that there is an enhanced deacceleration resulting in an enhanced offshore moisture flux convergence (neglecting a diurnal oscillation of the regional maritime low-level flow) that provide the low-level support for long-lived MCSs and newer storms development. These sequence of events agree well with those presented in the modeling studies of Mapes et al. (2003) and Yepes at al. (2020), and those shown in TRMM-based MCSs of Jaramillo et al. (2017).

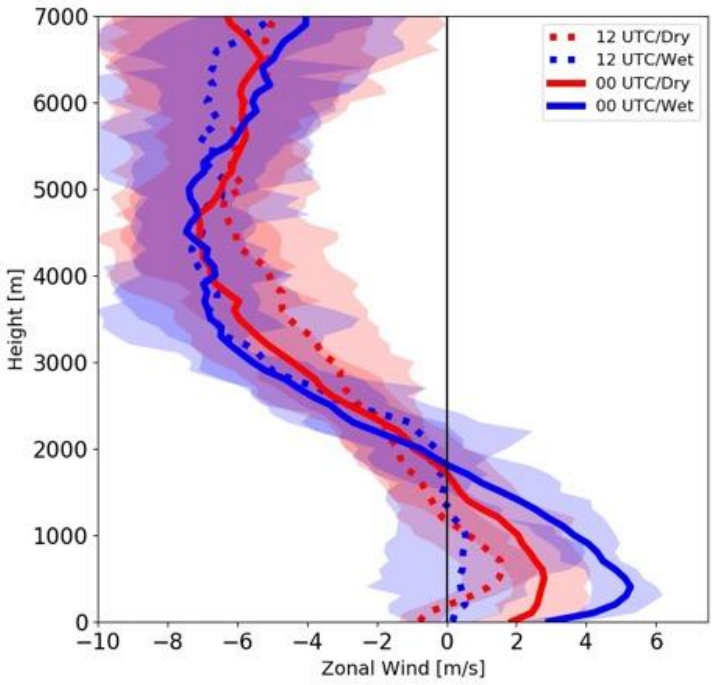

Figure 5 OTREC-Nuquí (August-September, 2019) zonal wind vertical composites during convectively active (Wet) and no convective (Dry) days and further composited by launching times 00 UTC (late afternoon) and 12 UTC (early morning). See text for characterization of wet/dry days. Shades show the interquartile range of each composite sample.

It is worth noticing that the inland precipitation maximum can be also related to the enhanced afternoon surface and boundary layer fluxes by the tropical rainforest located between the western range of the Andes and the Pacific shoreline. Tropical forests exhibit a clear-cut diurnal cycle of evapotranspiration and biogenic activity including the emission of volatile organic compounds (Gu et al., 2017) that get converted into cloud condensation nuclei. Also, such a diurnal cycle is associated with processes such as latent and sensible heat fluxes near the surface (evaporative cooling from the forest transpiration and from reevaporation of water intercepted and held by the vegetation) and condensation heating aloft. Another source of surface cooling lies in the high aerodynamic conductance of the forest, more so during Dry days, which constitutes the main surface cooling factor (Panwar et al., 2020; Davin and de Noblet-Ducoudré,

2010; Boisier et al., 2012; Lejeune et al., 2015). All these processes play an important role in the dynamics of atmospheric turbulent transfer within the boundary layer and therefore on the development and life cycle of convective processes in the region. This is a topic of on-going research.

3.2.2 Regional Patterns

To derive regional scale circulation changes related to Wet and Dry convection activity, the ERA5 reanalysis data are used. Recall that some confidence is gained in the ERA5 products as most *in situ* upper-air data were assimilated on real-time. For completeness and to address potential ERA5 uncertainties in this sparse data area, we also composited surface station observations made available by DIMAR. ERA5 and DIMAR observations agree generally well, with a few particular exceptions. For example, Malpelo island (4.002577 °N, 81.60429 °W) shows Wet minus Dry differences that are offset in relation to ERA5. We attributed such differences to surface station siting issues: Malpelo is a small rocky island that perturbs the circulation as the station is located (for practical reasons) in the lee side relative to the predominant flow (DIMAR personal communications). We assume, however, that ERA5 products over EPAC are relatively well-constrained by surface observations due to the high ship traffic in the area (Gallego et al., 2019).

Figure 6 shows the prevailing surface flow during the OTREC period, with westerly-southwesterly flow dominating over the far EPAC and easterly flow over the Caribbean basin. The confluence zone of these two broad and coherent circulation features form the ITCZ over the far EPAC. The northerly flow over Panama is known as

500 the Isthmus gap flow and typically flows from the Caribbean into the far EPAC this time
501 of the year, with a return component from the far EPAC to Northern Colombia over the
502 Colombia-Panama border. The latter low-level cyclonic circulation feature is known as
503 the Panama Bight semi-permanent low (Chelton et al., 2000; Rodríguez - Rubio et al.,
504 2003; hereafter Panama low). Figure 6c and f show that this surface circulation pattern is
505 more accentuated during Wet days (more so during the nighttime and early morning):
506 The Panama low is more pronounced, which might enhance surface convergence owing
507 to stronger easterlies over the Caribbean and stronger south westerlies over the EPAC.
508 The enhanced cyclonic flow related to Wet days and located to the NW of Nuquí
509 reinforces the idea of a stronger convergence zone just offshore during the morning
510 precipitation burst. Again, the enhanced convergence patterns are related to early
511 morning deacceleration of ChocoJet as revealed by the Nuquí observations (Figure 5).

512 Figure 7 shows the Panama low extending vertically and underscoring the
513 modification produced by its orography; this feature disappears above 800 hPa where the
514 easterly flow dominates (not shown). Over the far EPAC, the low-level circulation
515 (Figure 7a, b) clearly depicts the Panama Isthmus gap flow and ChocoJet confluence
516 zone wrapping cyclonically offshore the Colombia-Panama border. During Wet days,
517 defined as days with long-lasting organized convection, the ERA5 composites show an
518 accentuated cyclonic curvature suggesting that a thermodynamical adjustment could have
519 contributed to the lowering of the pressure produced by the storms. A momentum and
520 vorticity budget can help elucidate better the dominant forces in place. A similar
521 cyclonic pattern was found by Zuluaga and Houze (2015) and Liu et al. (2020) when
522 examining the environmental conditions driving convection organization and high-flash-

rete thunderstorms over the Northern Andes. This cyclonic curvature is shifted north from the one found in Zuluaga and Houze (2015), and it is collocated with the positive anomalies of rain shown in Figure 1d. Figure 7c and f show Wet minus Dry differences highlighting the low-level enhanced southwesterly flow over Pacific and Caribbean coasts of Colombia, which moves around the northern flank of the Andes and into the Magdalena River Valley (central Colombian valley). These results correspond well to those presented by Liu et al. (2020), who found that moisture surges moving from the far EPAC into the Northern Andes help increase both low-level moisture flux convergences and low-level bulk shear into the region. It is worth noticing the spatial coherence of the Wet minus Dry flow differences indicating that a stronger CLLJ appears to be related to Wet days. Over the Caribbean Sea, the CLLJ intensity is modulated by TEWs (Serra et al., 2010) which are seemingly sources of synoptic variability in the area. The coherence patterns between Wet days and TEWs incursions over the Caribbean is currently being addressed in a separate study.

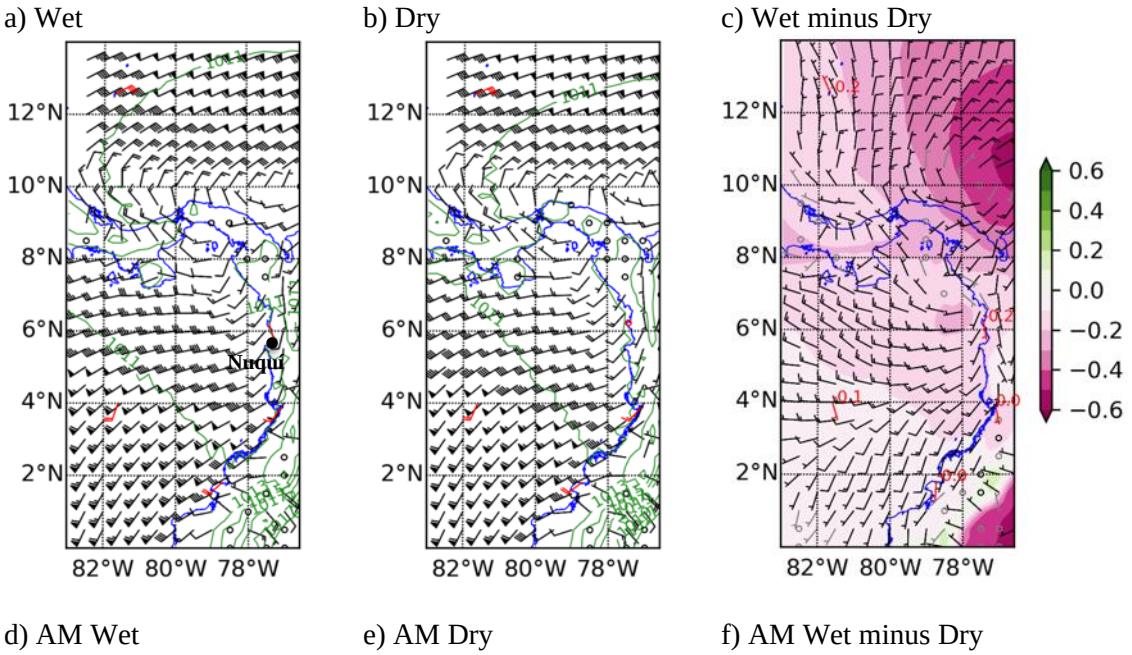

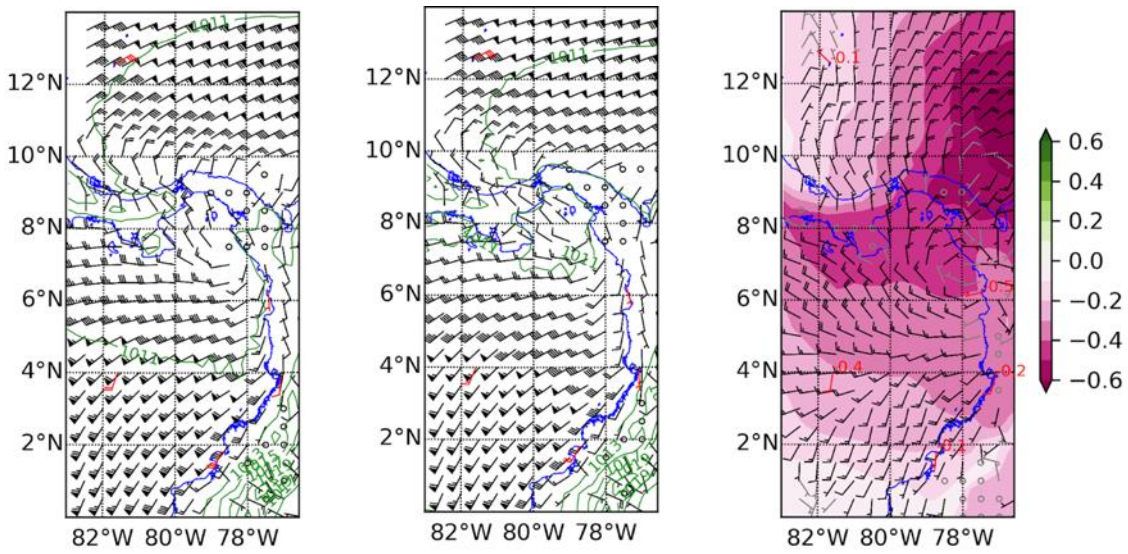

537 Figure 6 Surface ERA5 and DIMAR station composites for wind vectors and sea-level pressure (contours)
538 during OTREC (August-September, 2019) for (a) convectively active days (Wet), (b) non convective days
539 (Dry) and (c) Wet minus Dry differences; (d-f) for nighttime and early morning times only (00-08 LST; 05-
540 13 UTC). Black wind barbs correspond to ERA5 (subsample every other grid point), red bards correspond
541 to DIMAR stations. For Wet and Dry, full wind barb is 1 m/s, half is 0.5 m/s, flag is 5 m/s; For Wet minus
542 Dry, full barb is 0.5 m/s, half is 0.1 m/s. Bold barbs in (c) show differences that are statistically significant
543 with a 95% confidence level. Shaded contours represent ERA5 SLP differences (hPa) and red numbers next
544 to station locations are observed SLP differences in hPa. Coastline is shown in blue.

545

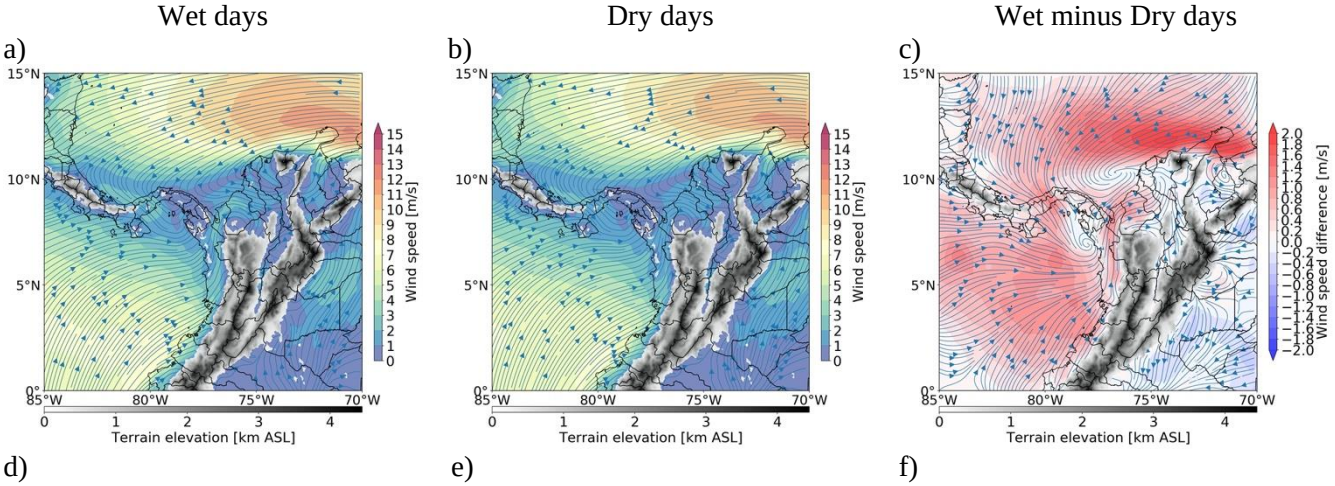

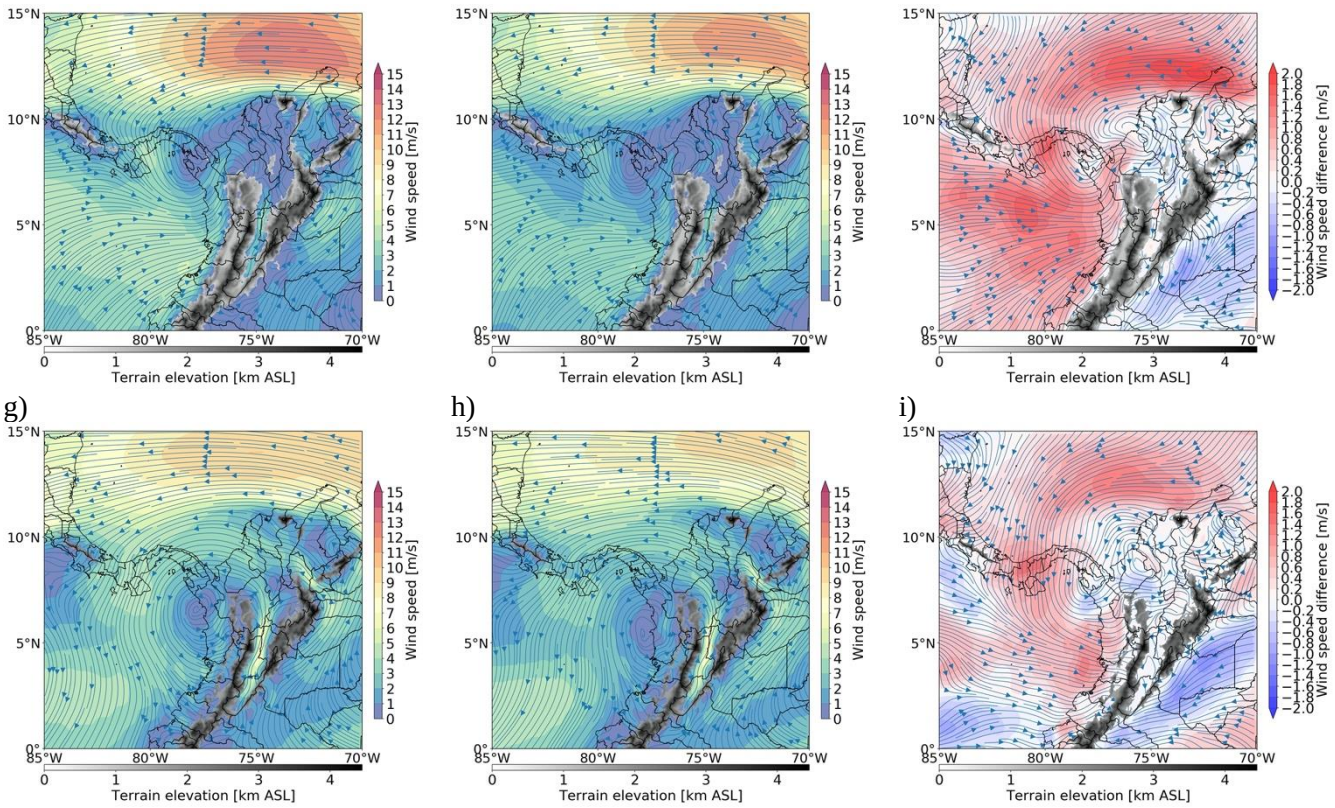

Figure 7 ERA5 pressure level circulation and wind speed composites during OTREC (August-September, 2019) for 975, 925, and 850 hPa during convectively active days (Wet), non-convective days (Dry) and Wet minus Dry day differences. Topography is also included above the corresponding pressure level (using a hydrostatic approximation) for reference of the flow and topography interaction.

3.3 Wind Shear

Both the ChocoJet and the easterly winds above the Andes were significantly more intense during Wet days (Figure 5), which suggests the existence of a vertical shear environment capable of controlling convection organization into MCSs. In this study, low-level wind shear is defined as the magnitude of the difference vector between ChocoJet (500-750 m ASL) and the lowest level at which easterly trade winds reach their maximum intensity (3000-3500 m ASL). Figure 8a shows that ChocoJet wind speed discriminates Wet from Dry days (99% confidence level) and is a good environmental factor of convection organization and precipitation amount, whereas the relationship of the mid-level wind speed and shear (Figure 8b and c) from the Wet and Dry days is

relatively weaker (only to the 80% confidence level). Although the shear-convective regime is not monotonically increasing, it suggests that a critical vertical shear of 10 and 14 m s^{-1} is needed for days with organized and persistent convective systems. It is worth noticing that this result is sensitive to the shear definition (i.e., Markowski and Richardson, 2006) and the significance of the relationship is given by the selection of the shear layers, leading to different shear critical values and variance in the significance of the relationship (Chen et al., 2015). Nevertheless, the directionality of the results was consistent, indicating that the environmental vertical shear induced by the Andes and the mid-tropospheric jet modulate convection organization into MCSs. The influence of the environmental vertical shear agrees well with previous studies in the area (Mejía and Poveda, 2005); a similar shear environment has been linked to high population of MCSs over the Sierra Madre Occidental (Mejía et al., 2016); interaction of a similar low-level vertical shear with convective outflows support long-live midlatitude and tropical squall lines (Rotunno et al., 1988; Weisman and Rotunno, 2004). Diurnally, Yepes et al. (2020) also pointed out the role of wind shear in the development of thunderstorms during early morning over this region. The role of vertical wind shear, which is observable and predictable, is encouraging.

The resultant down shear vector (not shown) is mainly westward owing to the strength of the easterlies, which helps support the westward propagating precipitation patterns shown in Figure 2Figure 3 and Figure A-1. The vertical shear is important as it interacts with low-level vorticity generated by the convective outflows helping develop new convective cells or maintain the existing ones (Markowski and Richardson, 2006). The observed vertical shear and its relationship to convection organization suggest that

583 vertical vorticity can be tilted and stretched by deep convection and support the
584 development of Mesoscale Convective Vortices (Davis and Galarneau 2009), which
585 constitutes yet another well-known dynamic support for long lasting MCSs (Weisman
586 and Rotunno, 2004; Hagos et al., 2013; Chen et al., 2015). A case study of an MCS
587 observed during OTREC will be presented later as an effort to strengthen and reconcile
588 the multiple ingredients in this composite work.

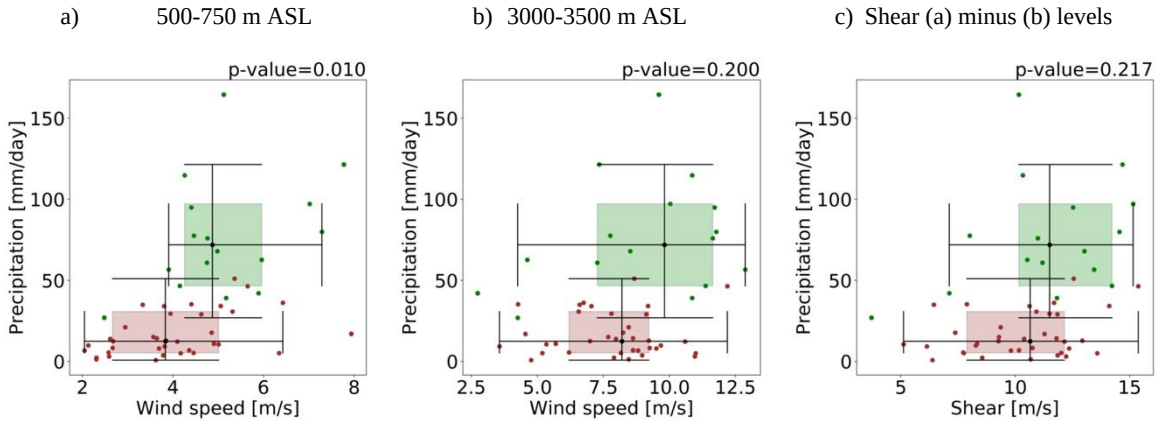

589 Figure 8 Scatter plots for OTREC daily precipitation total during the Wet (Green dots) and Dry (Brown)
590 days against (a) low-level (500-700 m ASL) or ChocoJet wind speed, (b) mid-level (3000-3500 m ASL) or
591 easterly trade wind speed, and (c) vertical shear estimated as the magnitude of the vector differences
592 between levels used in (a) and (b). Box plots show the median, interquartile range and extreme distribution
593 of the samples for each axis. P-values in the upper-right corner of each panel were only estimated for the
594 independent parameters (x-axis) evaluating the significance of the independence of the Wet and Dry
595 samples using the Student's t-test.

596 **3.4 On Gravity Waves**

597 To support the observed early morning and offshore precipitation maximum shown in
598 Figure 2, we now examine the thermodynamic profile and its relationship to the gravity
599 wave phenomenon. Using soundings from ChocoJEX, Yepes et al. (2019) and Yepes et
600 al. (2020) found a nighttime and early morning cold temperature disturbance between
601 800-600 hPa, likely related to the gravity wave phenomenon postulated by Mapes et al.
602 (2003). OTREC-Nuquí field campaign further supports this finding with a longer data

603 record. Figure 9 shows the mean Moist Static Energy (MSE) and Saturated MSE
604 (SMSE) diagrams measured during both ChocoJEX IOP3 in Quibdó (2016) and OTREC-
605 Nuquí. Despite the differences in location (Quibdó is located 65 km inland to the east of
606 Nuquí) and interannual and seasonal differences (not shown), both observation sites show
607 similar thermodynamic and diurnal characteristics, including: a built-up SMSE inversion
608 layer at 00 UTC (19 LT) and low-level stable conditions (surface to 800 hPa) at 12 UTC
609 (07 LT). Additionally, observations suggest that the cold phase of the gravity wave
610 erodes the SMSE inversion and increases the mid-level convection potential.
611 To better characterize the diurnal thermodynamical contrast, Figure 9c and d show
612 OTREC-Nuquí mean 12 UTC minus 00 UTC differences for θ and SMSE, respectively.
613 Results show pronounced 900 to 400 hPa early morning cool layers collocated with the
614 enhanced SMSE. A striking result is that Wet days are characterized by a more
615 pronounced middle-layer diurnal thermal difference, with its corresponding more
616 unstable thermodynamic profile. Hence, the timing and day-to-day variance of the cold
617 phase of the mid-level gravity wave mechanism consistently supports the potential
618 occurrence of an offshore precipitation maximum.
619 It is possible that some kind of cold advection and propagating phenomenon from the
620 Andes support such diurnal middle-level thermal contrast. Since we cannot attribute to
621 other phenomena and results support the idea of a gravity wave mechanisms that favor an
622 afternoon combination of advection and propagation of warm air over the Andes that
623 helps to build the observed inversion layer. This picture is completed by the nighttime
624 middle-level cooler air that helps erode the inversion, while enhancing the convective
625 potential energy aloft. Recall that Wet days are related to enhanced mid-level easterlies,

626 which can support enhanced thermal advection, with everything else assumed the same
627 (Figure 5). Rydbeck et al. (2017) modeling study found that westward moving MCSs
628 ceased when the Andes were removed, underscoring the importance of the gravity wave
629 produced by high rise topography. They acknowledge, however, that removing the
630 Andes can modulate the base state of other features highlighted here as crucial drivers in
631 the formation of MCSs and the precipitation hotspot, including the vertical shear, the
632 intensity of the land-breeze, the afternoon convection near the coast, and the intensity and
633 location of the CLLJ and ChocoJet.
634 It is possible that the westward extent of the gravity wave helps explain the relatively
635 long distance travelled by the offshore migration of convective systems during Wet days
636 (Figure 2). Using offshore upper-air soundings launched from a ship vessel, Yepes et al.
637 (2019) showed that the effect of the outlined gravity wave persists several hundred
638 kilometers offshore. However, there are other plausible mechanisms that can explain the
639 relatively long extent of the westward migration of the offshore precipitation. In
640 Sumatra, Yokoi et al. (2017, 2019) suggested that inland afternoon convection can help
641 activate gravity waves that can possibly play a role in the offshore migration of
642 precipitation. Idealized simulations for flat islands (Coppin and Bellon, 2019a) or islands
643 with mountains (Coppin and Bellon, 2019b) suggest that land breeze-related convection
644 can propagate far from the coast by the formation of mid-tropospheric gravity waves that
645 can trigger new convection or reinforce existing convection. They suggested that the
646 distance of propagation away from the shore is particularly sensitive to humidity and
647 temperature at the top of the boundary layer, citing the gravity wave phenomenon (Mapes
648 et al., 2003) as a plausible mechanisms in such sensitivity. All of these studies highlight

649 the role of gravity wave displacements as modulators of the nighttime and early morning
650 convective activity of their surroundings.

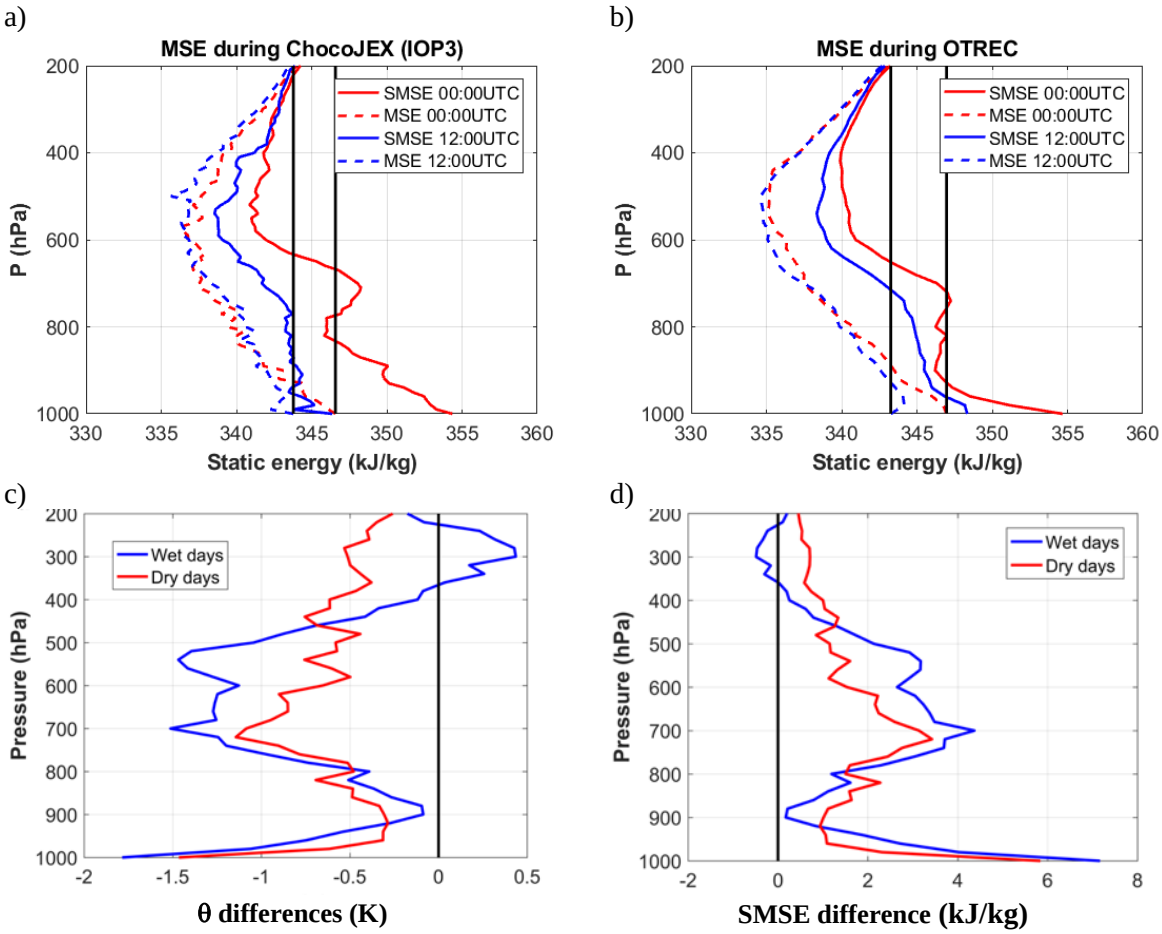

651 Figure 9 Mean Moist Static Energy (MSE) diagrams during (a) ChocoJEX (Quibdó, October 2016) and (b)
652 OTREC-Nuquí (August-September 2019; right) average at 00 UTC (19 LT) and 12 UTC (07 LT); Dotted
653 and Solid lines show the MSE and saturated MSE (SMSE), respectively. Mean OTREC Wet and Dry days
654 composites of (c) θ and (d) SMSE 12 minus 00 UTC differences.

655 ## 3.5 August 11th, 2019 MCS

656 To illustrate and further reinforce the role of circulation processes and
657 thermodynamics in the generation of precipitation and convection organization outlined
658 above, Figure 10 shows the dropsonde 3DVAR (Fuchs-Stone et al., 2020) temperature,
659 circulation and vorticity analysis based on the OTREC dropsonde observations released
660 from the NSF/NCAR Gulfstream V during the morning of August 11, 2019 (Voemel,

2019). During the day of the flight, an MSC (Wet day) developed inland early morning, and then moved offshore due west persisting until past noon. For reference, GOES brightness temperature, GPM precipitation totals, and wind barbs from 12 and 18 UTC Nuquí sounding are also shown. At low-level (Figure 10f, 950 hPa) streamline and temperature analysis show a confluence line (and low-level convergence around 5.5° N) separating two distinct air masses, the relatively cooler ChocoJet and the warmer Isthmus gap flow. At this level, southwesterly flow is much stronger than reported by the Nuquí sounding, likely due to storm blocking or the demise of the land breeze. This situation suggests low-level convergence over the eastern side of the flight pattern. Flow veered with height reaching a persistent easterly component just above the Andes (Figure 10c, 650 hPa) and underscoring the existing low-to-mid level environmental shear.

The dropsonde analysis clearly resolved what appears to be a coherent MCV between 650 and 300hPa (Figure 10a and Figure 11a). This MCV pattern, however, shows two distinctive layers with an onion-shaped thermodynamic profile in the upper half (300-450 hPa), with collocated cold and warm temperature anomalies above and below, respectively. This characteristic is indicative of the MCV cyclonic support in mid-levels to the related subsidence produced by the stratiform region of the MCSs (Figure A-2). Figure 12a show that the outlined convective system was dominated by a top-heavy mass profile, indicative of strong stratiform precipitation (Fuchs-Stone et al., 2020). The lower half of the MCV developed in a moist layer above the warmer and drier easterlies. We speculate that the deep cyclonic vorticity layer (4-9 km; Figure 12b) may be the result of stretching associated with the vertical mass flux profile, as suggested by the net mass flux increasing strongly with height, which implies horizontal mass convergence. Other flow

conditions are likely to contribute to the cyclonic shear, such as the perturbed flow by the wake zone related to upstream convective blocking, as evidenced by the flow around the southernmost deep convective cells, or event tilting of the sheared environment. Future research will perform a vorticity budget to examine the relative importance of the outlined mechanisms for this and other OTREC research flights and using cloud-resolving modeling tools.

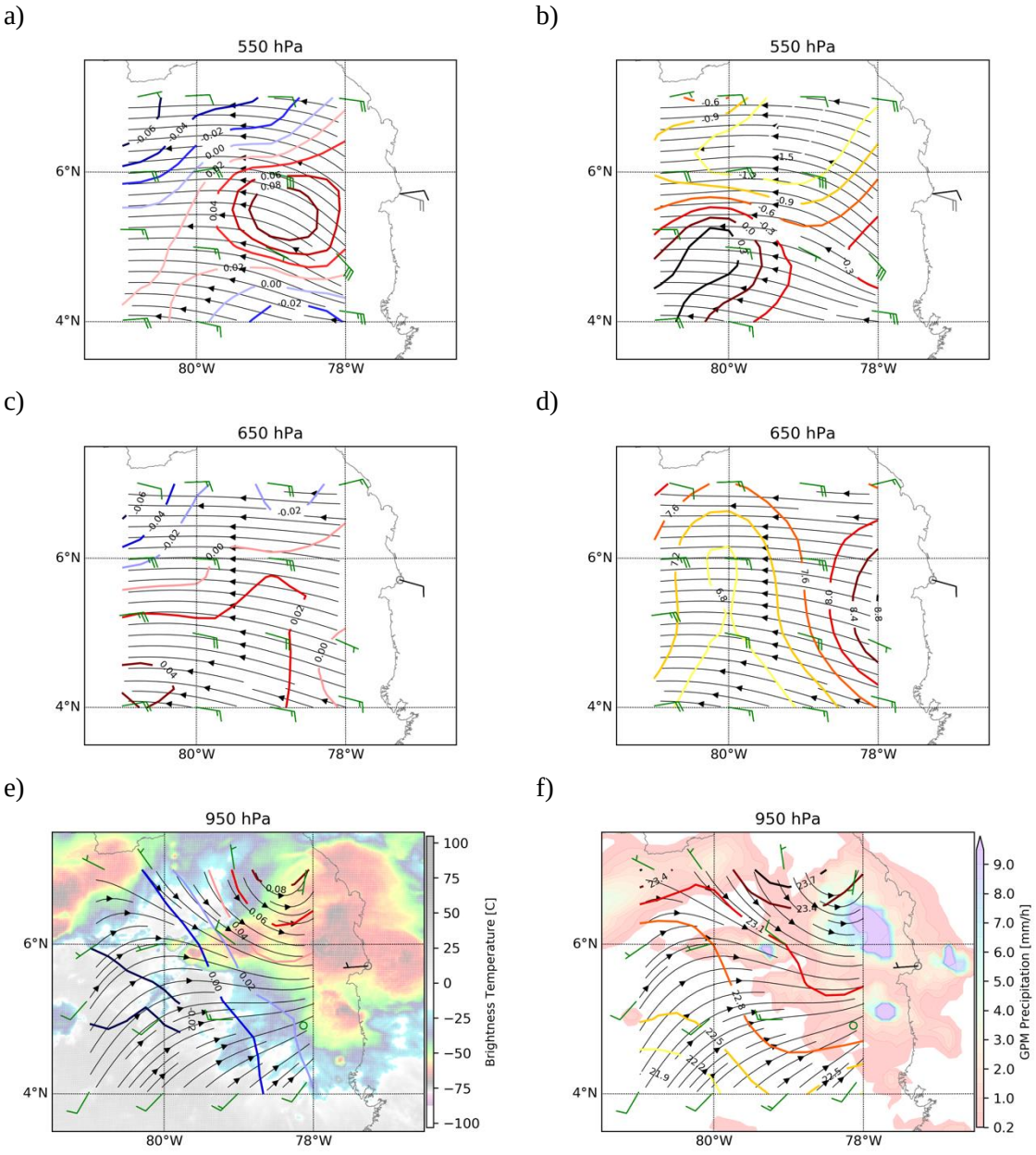

Figure 10 MCSs event during August 11, 2019 and 3DVAR contours of relative vorticity (left panels; s^{-1}) and temperature (right panels; °C) at 550, 650 and 950 hPa pressure levels. Streamlines and wind vectors at the dropsonde release location (green) and Nuquí soundings at 12 UTC (grey) and 18UTC (black) are included in each panel. Background imagery corresponds to GOES channel 14 at 15 UTC (bottom-left panel) and GPM IMERGv6 accumulated precipitation for 13-18 UTC (bottom-right panel). Different pressure levels and the dropsonde 3DVAR (Fuchs-Stone et al., 2020) temperature, circulation and vorticity analysis based on the OTREC dropsonde observations released from the NSF/NCAR Gulfstream V during the morning of August 11, 2019.

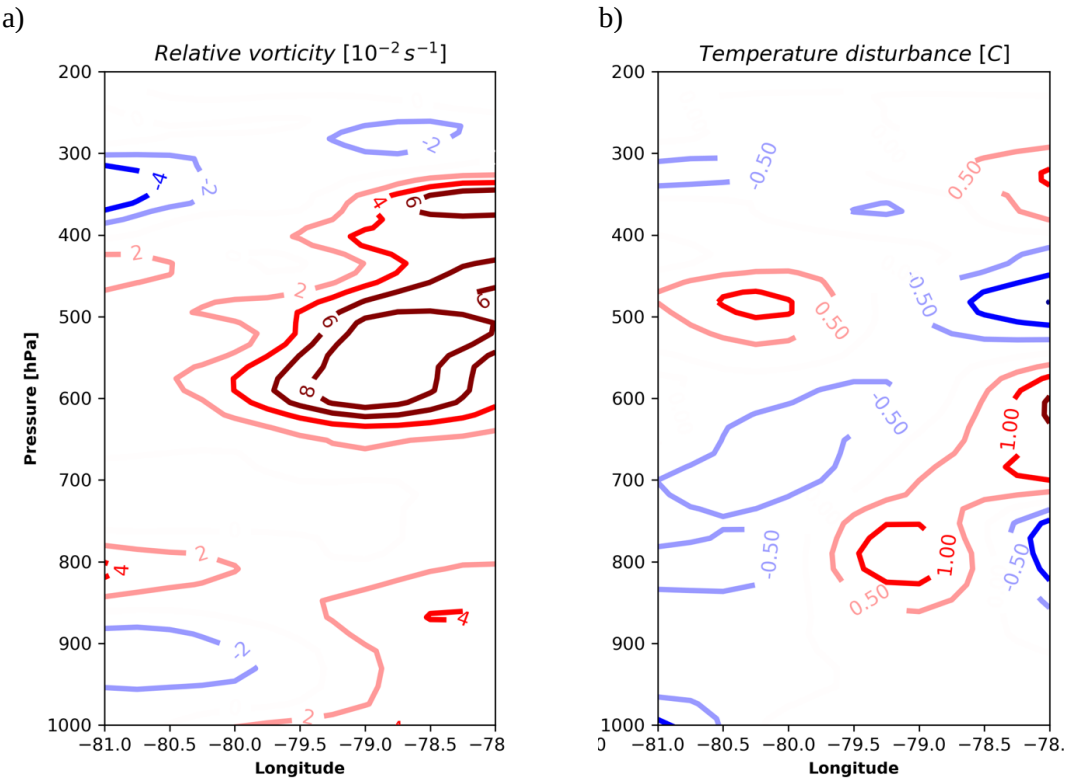

Figure 11 Longitude-pressure 3DVAR analysis for (a) relative vorticity (s^{-1}) and (b) temperature disturbance (ºC) at 5.5 ºN for flight shown in Figure 10.

a) b)

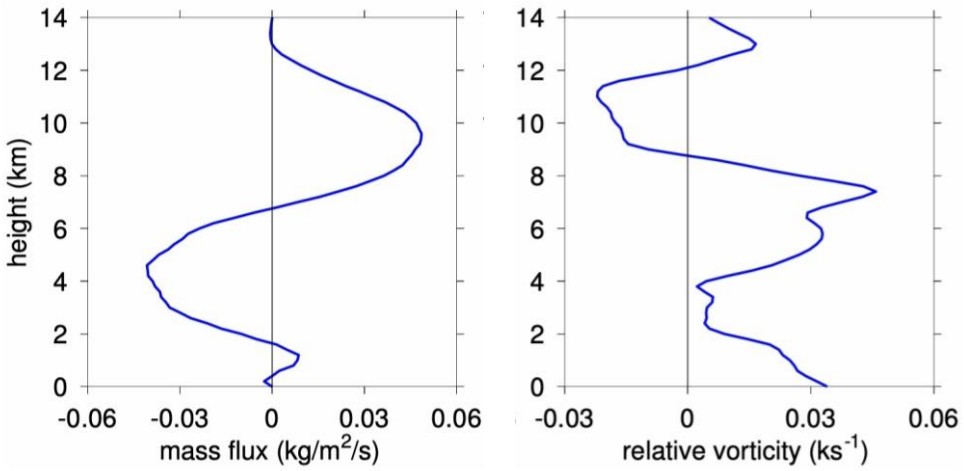

Figure 12 Vertical profile of 3DVAR analysis for (a) vertical max flux (kg m^{-2} s^{-1}) and (b) relative vorticity (ks^{-1}) spatial averaged (78-80º W, 5-7º N) for flight shown in Figure 10.

4 Summary and Conclusions

This study uses new observations gathered during Organization of Tropical East Pacific Convection (OTREC; August-September, 2019) to better understand the mechanisms responsible for the precipitative systems that occur in the rainiest spot on Earth, according to GPM data annual totals. We examined upper-air soundings observations launched at Nuquí, a Colombian coastal town located at the far EPAC and near the record-breaking precipitation maximum.

Associated with this record maximum is a pronounced nighttime and early morning diurnal precipitation distribution mostly falling in the form of recurrent and long lasting MCSs, predominantly moving westward from the Andes to several hundreds of kilometers into the ocean. OTREC-Nuquí field campaign was long enough (51 days) to develop robust statistical composites of the local and regional environment related to the development or reinforcement of MCSs.

We examined the local and regional environmental drivers modulating the circulation and thermodynamics during several MCS days. Additionally, a mesoscale analysis of an

individual MCS event observed during one of the OTREC GV research flights helped reinforce such connections. Both the composite analysis and mesoscale analysis provided an interesting set of mechanisms, not necessarily complete, that help understand the convective forces that can trigger, control their diurnal variance, or support MCS duration, which we now summarize:

- *ITCZ*: Enhanced low-level convergence formed by the ChocoJet and Panama gap jet, which constitute the ITCZ over the far EPAC. Orographic blocking help create the semi-permanent low that cyclonically wraps the ITCZ near the Colombian coast. This process seems to be regionally modulated by CLLJ and ChocoJet intensity.
- *Land breeze*: Land breeze favors ChocoJet deceleration offshore, enhancing the nighttime and early morning low-level convergences.
- *Vertical wind shear*: Sheared flow provides vertical dynamical support (Rotunno et al., 1988). This shear can interact with the low-level vorticity (generated by gravity currents and outflows) to further support upper motion and the down shear motion (predominantly westward). Days with stronger shear than average correlate well with organized and persistent convective systems.
- *Mid-level gravity wave*: Previous studies and the observations made here helped confirm the existence of the interaction of a gravity wave emanating from the Andes (Mapes et al., 2003). During the nighttime and early morning, the cold phase of the gravity wave enhances convection potential and helps erode the inversion layer that forms in the interface of the cold and moist EPAC airmass and the drier and warmer easterly airmass that flows above the Andes. More

research is needed to pinpoint the sources of the gravity wave and its corresponding propagating characteristics.

- *MCV*: Dropsonde observations show evidence of a well-organized MCV that developed during the occurrence of an MCS. Mid-level MCVs support upward motion than can help maintained and invigorate their parent MCS. This mid-level vorticity is most likely generated by stretching of ambient vorticity by the top-heavy vertical mass flux profile. We suggest that the combination of the vertical shear, the mid-level gravity wave and MCVs provide support for the maintenance and the relatively long distance travelled by the offshore convection. MCSs over the far EPAC constitute a source of local generation of mid-level vorticity that may contribute to downstream tropical cyclones development (Rydbeck et al., 2017).

This list of environmental and mesoscale drivers is by no means complete. We acknowledge that OTREC-Nuquí field campaign constitute an incomplete snapshot within the large annual and interannual variability of precipitation in the region. Future analysis of all OTREC G-V research flights is warranted, as is the analysis on *how* representative are the outlined mechanisms in the annual cycle context.

It is likely that synoptic-to-interannual variability of precipitation in the region is modulated through one or several of the outlined mechanisms. However, it is also likely that additional mechanisms are added when synoptic or large-scale transients occur (e.g., 2-day wave, TEW, MJO, etc.). Convection organization and spatial distribution is clearly modulated by the TEWs. Hence, a more in-depth analysis of variance added by synoptic

disturbances (including TEWs) can help us assess the roles of the far EPAC MCSs in triggering or amplification of easterly waves into tropical cyclogenesis in the core region.

The rainforest of the Chocó-Darién corridor between the western Andes and the Pacific coast of Colombia plays a fundamental role on the diurnal cycle through the supply of moisture from transpiration and reevaporation of intercepted rainfall and the ensuing surface evaporative cooling, but also cooling owing to the strong aerodynamic conductance of heat from the soil to the atmosphere (Davin and de Noblet-Ducoudré, 2010; Panwar et al., 2020), and their impact on the dynamics and thermodynamics of the boundary layer, convective processes and condensation aloft. The role of biogenic activity and remote aerosols (Riipinen et al., 2011; Bourgeois et al., 2015) in the clouds properties and precipitation of the region need to be investigated.

The results presented here can shed light about the mechanisms controlling the well-known large scale intraseasonal-to-seasonal teleconnection and variability drivers affecting the regional hydroclimate. Furthermore, the results provide hard observable and predictable constrains to global and regional models in the simulation of such outstanding precipitation hotspot. Note that several of the mechanisms in our list are model resolution dependent (e.g., land breeze, MCV). Hence, this list constitutes a recipe of basic environmental processes to diagnose and examine the fidelity and confidence in simulating MCSs in the region.

Acknowledgements: Support for this work was provided under NSF grant 1922918. Universidad Nacional de Colombia at Medellin, Colegio Mayor de Antioquia, and Universidad de Antioquia sponsored the time for OTREC-Nuquí participating students, while NSF funding sponsored all travel related expenses. We would like to acknowledge

operational, technical, and scientific support provided by NCAR's Earth Observing Laboratory, sponsored by the National Science Foundation. OTREC data are provided by NCAR/EOL under the sponsorship of the National Science Foundation https://data.eol.ucar.edu/project/OTREC. Data is available through Mejia and Poveda (2020) and Voemel et al. (2019). Mejia and Yepes were supported by NSF grant 1922918. Henao received funding by the Colombian Administrative Department of Science, Technology and Innovation (COLCIENCIAS) under the National Doctoral Grant 727 (2015). Poveda's work was supported by Universidad Nacional de Colombia at Medellín. Raymond and Fuchs-Stone were supported by NSF grant 1758513. Zuluaga was supported by Patrimonio Autónomo Fondo Nacional de Financiamiento para la Ciencia, la Tecnología y la Innovación, Francisco José de Caldas (ref. 80740-128-2019). Special thanks to all OTREC-Nuquí participants and to DRI administration for facilitating this international field campaign. Administration personnel from Hotel Puerta del Sol, Nuquí (Patricia Lozano and Don Ramon) for their continue logistic support during the field campaign. We also thank NASA for providing GPM dataset, and DIMAR for sharing surface station observations in the region.

5 References

Amador, J. (2008), The Intra-Americas Sea low-level jet: overview and future research. *Annals of the New York Academy of Sciences, 1146*, 153–188. http://doi.org/10.1196/annals.1446.012

Arias, P.A., Martínez, J.A. & Vieira, S.C. (2015), Moisture sources to the 2010–2012 anomalous wet season in northern South America. *Clim Dyn, 45*, 2861–2884. https://doi.org/10.1007/s00382-015-2511-7

Arnett, A.B. & C.R. Steadman (1970), Low-level wind flow over eastern Panama and northwestern Colombia, ESSA Technical Memorandum ERLTM-ARL 26, U. S. Department of Commerce, Environmental Science Services Administration Research Laboratories, Air Resources Lab., Silver Spring, Maryland, 73 pp.

Baranowski, D. B., Waliser, D. E., Jiang, X., Ridout, J. A., & Flatau, M. K. (2019), Contemporary GCM fidelity in representing the diurnal cycle of precipitation over the Maritime Continent. *J. Geophys. Res. Atmos.*, *124* (2), 747-769.

Bedoya-Soto, J. M., Aristizábal, E., Carmona, A. M., and Poveda, G. (2019), Seasonal shift of the diurnal cycle of rainfall over Medellin's valley, central Andes of Colombia (1998–2005). *Front. Earth Sci.*, *7*:92. doi: 10.3389/feart.2019.00092

Biasutti, M., Yuter, S.E., Burleyson, C.D. et al. (2012), Very high-resolution rainfall patterns measured by TRMM precipitation radar: seasonal and diurnal cycles. *Clim Dyn*, *39*, 239–258. https://doi.org/10.1007/s00382-011-1146-6

Boisier, J., de Noblet-Ducoudré, N., Pitman, A., et al. (2012), Attributing the impacts of land-cover changes in temperate regions on surface temperature and heat fluxes to specific causes: results from the first lucid set of simulations. *J. Geophys. Res. Atmos.*, *117*(D12), 1-16.

Bourgeois, Q., Ekman, A. M. L., and Krejci, R. (2015), Aerosol transport over the Andes from the Amazon Basin to the remote Pacific Ocean: A multiyear CALIOP assessment, *J. Geophys. Res. Atmos.*, *120*, 8411–8425, doi:10.1002/2015JD023254.

Cárdenas, S. G., Arias, P. A., & Vieira, S. C. (2017), The African Easterly Waves over Northern South America. *In Multidisciplinary Digital Publishing Institute Proceedings* (Vol. 1, No. 5, p. 165)

Chelton, D.B., M.H. Freilich, and S.K. Esbensen (2000), Satellite Observations of the Wind Jets off the Pacific Coast of Central America. Part II: Regional Relationships and Dynamical Considerations. *Mon. Wea. Rev.*, *128*, 2019–2043, https://doi.org/10.1175/1520-0493(2000)128<2019:SOOTWJ>2.0.CO;2

Chen, Q., J. Fan, S. Hagos, W. I. Gustafson Jr., and L. K. Berg (2015), Roles of wind shear at different vertical levels: Cloud system organization and properties, *J. Geophys. Res. Atmos*, *120*, 6551–6574, doi:10.1002/2015JD023253.

Chong, M., & Bousquet, O. (1999), A mesovortex within a near-equatorial mesoscale convective system during TOGA COARE. *Mon. Wea. Rev.*, *127*(6), 1145-1156.

Christoplos, I., Rodríguez, T., Schipper, E.L.F., Narvaez, E.A., Bayres Mejía, K.M., Buitrago, R., Gómez, L. and Pérez, F.J. (2010), Learning from recovery after Hurricane Mitch. *Disasters*, *34*: S202-S219. doi:10.1111/j.1467-7717.2010.01154.x

Copernicus Climate Change Service (C3S): ERA5: Fifth generation of ECMWF atmospheric reanalyses of the global climate, Copernicus Climate Change Service Climate Data Store (CDS), available at: https://cds.climate.copernicus.eu/cdsapp#!/home, last access: 11 May 2020.

Coppin, D., & Bellon, G. (2019b), Physical mechanisms controlling the offshore propagation of convection in the tropics: 2. Influence of topography. *Journal of Advances in Modeling Earth Systems*, *11*, 3251– 3264. https://doi.org/10.1029/2019MS001794

Coppin, D., & Bellon, G. (2019a), Physical mechanisms controlling the offshore propagation of convection in the tropics: 1. Flat island. *Journal of Advances in Modeling Earth Systems*, *11*(9), 3042-3056.

Coppola, E., Giorgi, F., Raffaele, F. et al. (2014), Present and future climatologies in the phase I CREMA experiment. *Climatic Change, 125*, 23–38. https://doi.org/10.1007/s10584-014-1137-9

Davin, E.L., de Noblet-Ducoudré, N. (2010), Climatic impact of global scale deforestation: radiative versus nonradiative processes. *J. Climate, 23*(1), 97-112.

Davis, C.A. and T.J. Galarneau (2009), The Vertical Structure of Mesoscale Convective Vortices. *J. Atmos. Sci., 66*, 686–704, https://doi.org/10.1175/2008JAS2819.1

Dominguez, C., Done, J.M. & Bruyère, C.L. (2020), Easterly wave contributions to seasonal rainfall over the tropical Americas in observations and a regional climate model. *Clim Dyn, 54*, 191–209. https://doi.org/10.1007/s00382-019-04996-7

Drobinski, P., and Dubos, T. (2009), Linear breeze scaling: from large-scale land/sea breezes to mesoscale inland breezes. *Q. J. R. Meteorol. Soc.: A journal of the atmospheric sciences, applied meteorology and physical oceanography, 135*(644), 1766-1775.

Durán-Quesada, A. M., Reboita, M., and Gimeno, L. (2012), Precipitation in tropical America and the associated sources of moisture: a short review. *Hydrological sciences journal, 57*(4), 612-624.

Espinoza, J. C., Garreaud, R., Poveda, G., Arias, P. A.,Molina-Carpio, J.,Masiokas, M., et al. (2020), Hydroclimate of the Andes Part I: main climatic features. *Front. Earth Sci. 8*:64. doi: 10.3389/feart.2020.00064

Fuchs-Stone, Ž., Raymond, D. J., & Sentić, S. (2020), OTREC2019: Convection over the East Pacific and Southwest Caribbean. *Geophys. Res. Letts, 47*, e2020GL087564.https://doi.org/10.1029/2020GL087564

Gallego, D., García Herrera, R., Delgado, G., de Paula, F., Ordóñez Pérez, P., & Ribera, P. (2019), Tracking the moisture transport from the Pacific towards Central and northern South America since the late 19th century. *Earth system dynamics*, *10*(2), 319-331.

García-Martínez, I.M., Bollasina, M.A. (2020), Sub-monthly evolution of the Caribbean Low-Level Jet and its relationship with regional precipitation and atmospheric circulation. *Clim Dyn, 54*, 4423–4440. https://doi.org/10.1007/s00382-020-05237-y

Grau, H.R. and M. Aide (2008), Globalization and land-use transitions in Latin America. *Ecology and Society*, *13*(2), 16, www.ecologyandsociety.org/ vol13/iss2/art16/.

Gu D, Guenther AB, Shilling JE, Yu H, Huang M, Zhao C, Yang Q, Martin ST, Artaxo P, Kim S, Seco R, Stavrakou T, Longo KM, Tóta J, de Souza RAF, Vega O, Liu Y, Shrivastava M, Alves EG, Santos FC, Leng G, Hu Z (2017), Airborne observations reveal elevational gradient in tropical forest isoprene emissions. *Nat Commun., 8*:1–7. https://doi.org/10.1038/ncomms15541

Hagos, S., Z. Feng, S. McFarlane, and L. R. Leung (2013), Environment and the lifetime of tropical deep convection in a cloud-permitting regional model simulation, *J. Atmos. Sci., 70*, 2409–2425, doi:10.1175/jas-d-12-0260.1.

Hennon, Christopher C., Philippe P. Papin, Christopher M. Zarzar, Jeremy R. Michael, J. Adam Caudill, Carson R. Douglas, Wesley C. Groetsema et al. (2013), Tropical cloud cluster climatology, variability, and genesis productivity. *J. Climate, 26*, no. 10: 3046-3066.

Hersbach, H., and Coauthors (2020), The ERA5 Global Reanalysis. *Q. J. R. Meteorol. Soc.*, qj.3803, https://doi.org/10.1002/qj.3803.

Hidalgo, H.G., Durán-Quesada, A.M., Amador, J.A. and Alfaro, E.J. (2015), A Proposed Dynamical Mechanism Linking Pacific and Caribbean Climate. *Geografiska Annaler: Series A, Physical Geography, 97*: 41-59. doi:10.1111/geoa.12085

Houze, R. A. (2004), Mesoscale convective systems, *Rev. Geophys.*, 42, RG4003, doi:10.1029/2004RG000150.

Hoyos I., F. Dominguez, J. Cañón-Barriga, J. A. Martínez, R. Nieto, L. Gimeno and P. A. Dirmeyer (2018), Moisture origin and transport processes in Colombia, northern South America, *Clim Dyn*, 10.1007/s00382-017-3653-6, 50, 3-4, (971-990).

Huaman, L., and Takahashi, K. (2016), The vertical structure of the eastern Pacific ITCZs and associated circulation using the TRMM Precipitation Radar and in situ data. *Geophys. Res. Lett.*, *43*(15), 8230-8239

Huang, X., Hu, C., Huang, X. et al. (2018),A long-term tropical mesoscale convective systems dataset based on a novel objective automatic tracking algorithm. *Clim Dyn 51*, 3145–3159. https://doi.org/10.1007/s00382-018-4071-0

Huffman, G., Bolvin, D. T., Braithwaite, D., Hsu, K., Joyce, R., Kidd, C., Xie, P. (2018), NASA Global Precipitation Measurement (GPM) Integrated Multi-satellitE Retrievals for GPM (IMERG) Prepared for: Global Precipitation Measurement (GPM) National Aeronautics and Space Administration (NASA).

Jaramillo, L., G. Poveda, and J. F. Mejía (2017) Mesoscale convective systems and other precipitation features over the tropical Americas and surrounding seas as seen by TRMM. *Int. J. Climatol.*, *37*(S1), 380–397.

Kharin, V. V., Zwiers, F. W., Zhang, X. & Hegerl, G. C. (2007), Changes in temperature and precipitation extremes in the IPCC ensemble of global coupled model simulations. *J. Climate, 20*, 1419–1444.

King, M. J., M.C. Wheeler, and T. P. Lane (2017), Mechanisms linking global 5-day waves to tropical convection. *J. Atmos. Sci.*, *74*, 3679–3702, https://doi.org/10.1175/JAS-D-17-0101.1

Lejeune, Q., Davin, E.L., Guillod, B.P., and Seneviratne, S.I. (2015), Influence of Amazonian deforestation on the future evolution of regional surface fluxes, circulation, surface temperature and precipitation, *Clim Dyn*, 44, 2769–2786, doi:10.1007/s00382-014-2203-8.

Liu, N., C. Liu, B. Chen, and E. Zipser (2020), What Are the Favorable Large-Scale Environments for the Highest-Flash-Rate Thunderstorms on Earth?. *J. Atmos. Sci.*, *77*, 1583–1612, https://doi.org/10.1175/JAS-D-19-0235.1

Liu, W., Cook, K. H., & Vizy, E. K. (2019), The role of mesoscale convective systems in the diurnal cycle of rainfall and its seasonality over sub-Saharan Northern Africa. *Clim Dyn*, *52*(1-2), 729-745.

Loaiza Cerón, W., Andreoli, R.V., Kayano, M.T., Ferreira de Souza, R.A., Jones, C., Carvalho, L.M.V. (2020), The Influence of the Atlantic Multidecadal Oscillation on the Choco Low-Level Jet and Precipitation in Colombia. *Atmosphere*, *11*, 174.

Ma, J., Chadwick, R., Seo, K. H., Dong, C., Huang, G., Foltz, G. R., & Jiang, J. H. (2018), Responses of the tropical atmospheric circulation to climate change and connection to the hydrological cycle. *Annual Review of Earth and Planetary Sciences*, *46*, 549-580.

Mapes, B. E., T. T. Warner, and M. Xu (2003) Diurnal patterns of rainfall in northwestern South America. Part III: Diurnal gravity waves and nocturnal convection offshore. *Mon. Wea. Rev., 131*(5), 830–844.

Markowski, P., and Richardson, Y. (2006), On the classification of vertical wind shear as directional shear versus speed shear. *Weather and forecasting, 21*(2), 242-247.

Martinez, C., Goddard, L., Kushnir, Y. et al. (2019), Seasonal climatology and dynamical mechanisms of rainfall in the Caribbean. *Clim Dyn, 53*, 825–846 (2019). https://doi.org/10.1007/s00382-019-04616-4

Mejía, F., Mesa, O., Poveda, G., Vélez, J., Hoyos, C., Mantilla, R., ... and Cuartas, A. (1999), Distribucion Espacial y Ciclos Anual y Semianual de la Precipitacion en Colombia. *Dyna, 127*, 7.

Mejía, J. and Poveda, G. (2020), Upper-air Measurements at Nuquí, Colombia. Version 1.0. UCAR/NCAR - Earth Observing Laboratory. https://doi.org/10.26023/M951-SXZK-NF0N. Accessed 31 March 2020.

Mejía, J. F. and G. Poveda (2005) Ambientes Atmosféricos de Sistemas Convectivos de Mesoescala sobre Colombia durante 1998 según la misión TRMM y el re-análisis NCEP/NCAR. *Rev. Acad. Colomb. Cienc. 29* (113): 495-514. 2005. ISSN 0370-3908.

Mejía, J.F., Douglas, M.W. and Lamb, P.J. (2016), Observational investigation of relationships between moisture surges and mesoscale- to large-scale convection during the North American monsoon. *Int. J. Climatol., 36*: 2555-2569. doi:10.1002/joc.4512

Molinari, J. and D. Vollaro (2000), Planetary- and Synoptic-Scale Influences on Eastern Pacific Tropical Cyclogenesis. *Mon. Wea. Rev., 128*, 3296–3307, https://doi.org/10.1175/1520-0493(2000)128<3296:PASSIO>2.0.CO;2

Murakami, H., Wang, B., Li, T. et al. (2013), Projected increase in tropical cyclones near Hawaii. *Nature Clim Change 3*, 749–754. https://doi.org/10.1038/nclimate1890

Na, Y., Fu, Q., and Kodama, C. (2020), Precipitation probability and its future changes from a global cloud-resolving model and CMIP6 simulations. *J. Geophys. Res. Atmos., 125*, e2019JD031926. https://doi.org/10.1029/2019JD031926

Panwar, A., Renner, M., and Kleidon, A. (2020). Imprints of evaporation and vegetation type in diurnal temperature variations, *Hydrol. Earth Syst. Sci. Discuss.*, https://doi.org/10.5194/hess-2020-95, in review.

Poveda G, Espinoza JC, Zuluaga MD, Solman SA, Garreaud R and van Oevelen PJ (2020), High Impact Weather Events in the Andes. *Front. Earth Sci. 8*:162. doi: 10.3389/feart.2020.00162

Poveda, G. (2004), La hidroclimatología de Colombia: una síntesis desde la escala inter-decadal hasta la escala diurna. *Rev. Acad. Colomb. Cienc, 28*, 201–222.

Poveda, G., and O. J. Mesa (1999), La corriente de chorro superficial del oeste (del Chocó) y otras dos corrientes de chorro en Colombia: Climatología y variabilidad durante las fases del ENSO. *Rev. Acad. Colomb. Cienc, 89*, 517–528.

Poveda, G., and O. J. Mesa (2000), On the existence of Lloró (the rainiest locality on Earth): Enhanced ocean-land-atmosphere interaction by a low-level jet. *Geophys. Res. Lett., 27*, 1675–1678, https://doi.org/10.1029/1999GL006091. http://dx.doi.org/10.1029/1999GL006091.

Poveda, G., L. Jaramillo, and L. F. Vallejo (2014), Seasonal precipitation patterns along

pathways of South American low-level jets and aerial rivers, *Water Resour. Res.*, *50*, 98–118, doi:10.1002/2013WR014087

Poveda, G., O.J. Mesa, P.A. Arias, L.F. Salazar, H. Moreno, S.C. Vieira, P.A. Agudelo, V.G. Toro, and J.F. Álvarez (2005), Diurnal cycle of precipitation in the tropical Andes of Colombia. *Mon. Wea. Rev., 133*, No.1, pp. 228-240.

Poveda, G., P. R. Waylen, and R. Pulwarty (2006), Modern climate variability in northern South America and southern Mesoamerica. *Palaeogeogr. Palaeoclimatol. Palaeoecol., 234*, 3–27, https://doi.org/10.1016/j.palaeo.2005.10.031.

Raymond, D. J., Esbensen, S. K., Paulson, C., Gregg, M., Bretherton, C. S., Petersen, W. A., et al. (2004), EPIC2001 and the coupled ocean-atmosphere system of the tropical East Pacifc. *Bull. Amer. Meteor. Soc., 85*, 1341–1354.

Riipinen, I., et al. (2011), Organic condensation: A vital link connecting aerosol formation to cloud condensation nuclei (CCN) concentrations, *Atmos. Chem. Phys., 11*(8), 3865–3878, doi:10.5194/acp-11-3865-2011.

Roca, R., J. Aublanc, P. Chambon, T. Fiolleau, and N. Viltard (2014), Robust Observational Quantification of the Contribution of Mesoscale Convective Systems to Rainfall in the Tropics. *J. Climate, 27*, 4952–4958, https://doi.org/10.1175/JCLI-D-13-00628.1

Rodríguez-Rubio, E., Schneider, W., and Abarca del Río, R. (2003), On the seasonal circulation within the Panama Bight derived from satellite observations of wind, altimetry and sea surface temperature, *Geophys. Res. Lett., 30*, 1410, doi:10.1029/2002GL016794, 7.

Rotunno, R., J. B. Klemp, and M. L. Weisman (1988), A Theory for Strong, Long-Lived Squall Lines. *J. Atmos. Sci., 45*, 463–485, https://doi.org/10.1175/1520-0469(1988)045<0463:ATFSLL>2.0.CO;2.

Rueda, O. A. and G. Poveda (2006), Spatial and temporal variability of the Choco Low Level Jet and its effect on the hydroclimatology of the Colombian Pacific region. *Colombian Meteorology, 10*, 132–145. (Available in Spanish).

Ruppert Jr, J. H., & Zhang, F. (2019), Diurnal Forcing and Phase Locking of Gravity Waves in the Maritime Continent. *J. Atmos. Sci., 76*(9), 2815-2835.

Rydbeck, A. V., Maloney, E. D., & Alaka Jr, G. J. (2017), In situ initiation of east Pacific easterly waves in a regional model. *J. Atmos. Sci., 74* (2), 333-351.

Sakamoto, M. S., T. Ambrizzi, and G. Poveda (2011), Moisture sources and life cycle of convective systems over western Colombia. *Advances in Meteorology, 2011*, 1–11. http://doi.org/10.1155/2011/890759

Schneider, E. K., Lindzen, R. S. & Kirtman, B. P. (1997), A tropical influence on global climate. *J. Atmos. Sci. 54*, 1349–1358.

Serra, Y., G. Kiladis, and K. Hodges (2010), Tracking and mean structure of easterly waves over the Intra-Americas Sea. *J. Climate, 23*, 4823–4840.

Snow, J. W. (1976), The climate of northern South America. Climates of Central and South America. W. Schwerdtfeg, Elsevier, 295-403.

Tan, J., Huffman, G. J., Bolvin, D. T., & Nelkin, E. J. (2019), Diurnal cycle of IMERG V06 precipitation. *Geophys. Res. Lett., 46*, 13584– 13592. https://doi.org/10.1029/2019GL085395

Tang, G., Clark, M. P., Papalexiou, S. M., Ma, Z., and Hong, Y. (2020), Have satellite precipitation products improved over last two decades? A comprehensive comparison of GPM IMERG with nine satellite and reanalysis datasets. *Remote Sensing of Environment*, *240*, 111697.

Vallejo-Bernal, S.M., Urrea, V., Bedoya-Soto, J.M., Posada, D., Olarte, A., Cárdenas-Posso, Y., Ruiz-Murcia, F., Martínez, M.T., Petersen, W.A., Huffman, G.J. and Poveda, G. (2020), Ground Validation of TRMM 3B43 V7 Precipitation Estimates over Colombia. Part I: Monthly and Seasonal Timescales. *Int J Climatol.*, doi:10.1002/joc.6640

Velasco, I., and Fritsch, J. M. (1987) Mesoscale convective complexes in the Americas. *J. Geophys. Res. Atmos.*, *92*, 9591–9613. doi: 10.1029/JD092iD08p09591

Voemel, H. (2019), NCAR/EOL AVAPS Dropsonde QC Data. Version 1.0. UCAR/NCAR - Earth Observing Laboratory. https://doi.org/10.26023/EHRT-TN96-9W04. Accessed 13 January 2020.

Wang, S., and Sobel, A. H. (2017), Factors controlling rain on small tropical islands: Diurnal cycle, large-scale wind speed, and topography. *J. Atmos. Sci., 74*(11), 3515-3532.

Warner, T. T., B. E. Mapes, and M. Xu, 2003: Diurnal patterns of rainfall in northwestern South America. Part II: Model simulations. *Mon. Wea. Rev.*, 131, 813–829.

Weisman, M. L., and R. Rotunno (2004), A theory for strong long-lived squall lines" revisited. *J. Atmos. Sci., 61*, 361–382.

Yang, G. and J. Slingo (2001) The Diurnal Cycle in the Tropics. *Mon. Wea. Rev., 129*, 784–801, https://doi.org/10.1175/1520-0493(2001)129<0784:TDCITT>2.0.CO;2

Yepes, J., G. Poveda, J. F. Mejía, C. Rueda and L. Moreno (2019) CHOCO-JEX: A Research Experiment Focused on the CHOCO Low-level Jet over the Far Eastern Pacific and Western Colombia. *Bull. Amer. Meteor. Soc.*, *100* (5), 779-796.

Yepes, J., J. F. Mejía, G. Poveda and B. Mapes (2020) Gravity waves modulating the diurnal cycle of precipitation over one of the rainiest spots on Earth: Observations and Simulations in 2016. *Mon. Wea. Rev.* (Accepted).

Yokoi, S., S. Mori, F. Syamsudin, U. Haryoko, and B. Geng (2019) Environmental Conditions for Nighttime Offshore Migration of Precipitation Area as Revealed by In Situ Observation off Sumatra Island. *Mon. Wea. Rev., 147*, 3391–3407, https://doi.org/10.1175/MWR-D-18-0412.1

Yokoi, S., S. Mori, M. Katsumata, B. Geng, K. Yasunaga, F. Syamsudin, Nurhayati, and K. Yoneyama (2017), Diurnal Cycle of Precipitation Observed in the Western Coastal Area of Sumatra Island: Offshore Preconditioning by Gravity Waves. *Mon. Wea. Rev., 145*, 3745–3761, https://doi.org/10.1175/MWR-D-16-0468.1

Yulihastin, E., Wahyu Hadi, T., Sari Ningsih, N., and Ridho Syahputra, M. (2020), Early morning peaks in the diurnal cycle of precipitation over the northern coast of West Java and possible influencing factors, *Ann. Geophys.*, *38*, 231–242, https://doi.org/10.5194/angeo-38-231-2020.

Zuluaga, M. D., and R. A. Houze (2015), Extreme convection of the near-equatorial Americas, Africa, and adjoining oceans as seen by TRMM. *Mon. Wea. Rev., 143*(1), 298–316. http://doi.org/10.1175/MWR-D-14-00109.1

6 Appendix

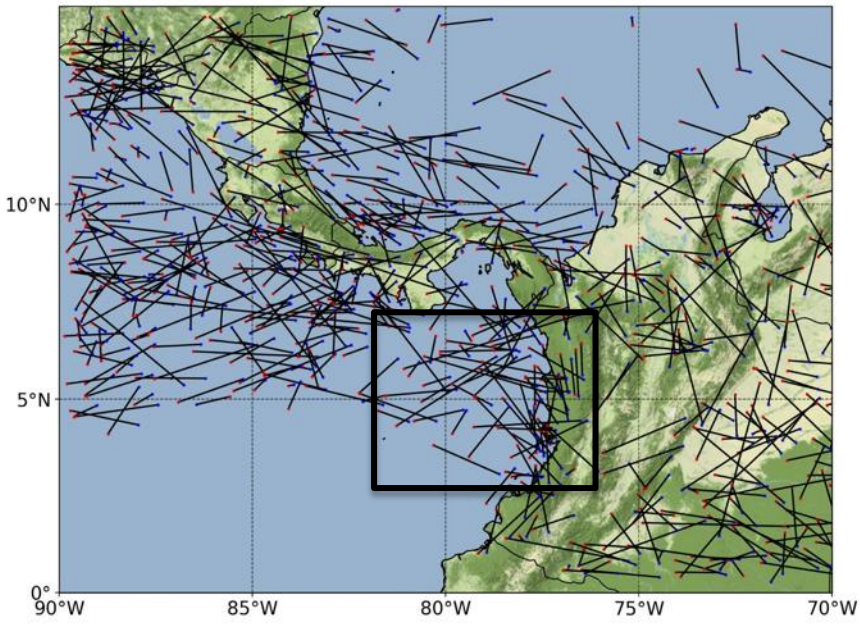

Figure A-1 GPM-based MSC trajectories lasting longer than 6 hours during OTREC as characterized by their initial (blue dot) and final (red dot) centroid locations.

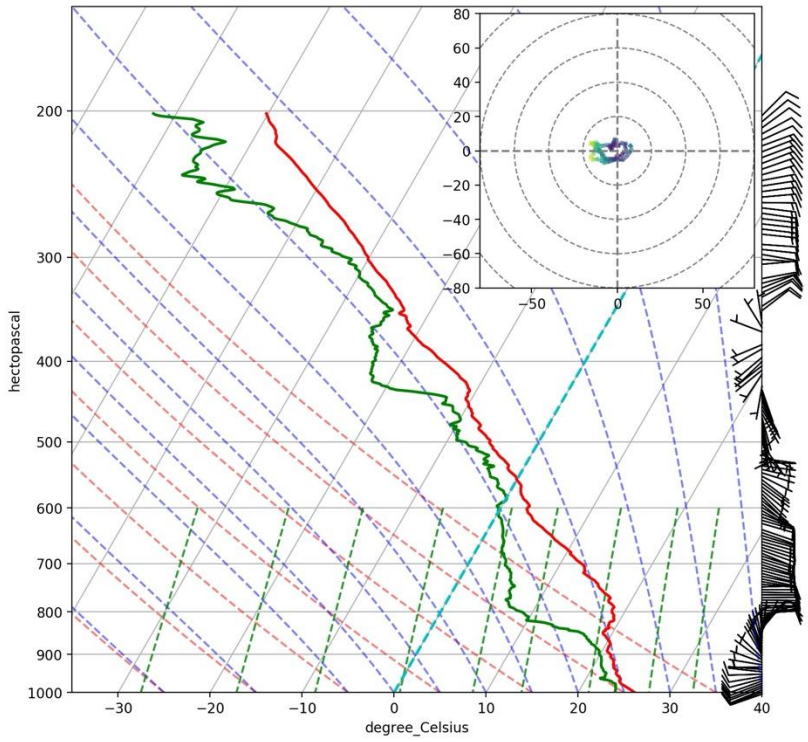

Figure A-2 Dropsonde Skew-T/log P diagram and wind profile corresponding to OTREC Research Flight 02 (2019-08-11) at 14:16 UTC.

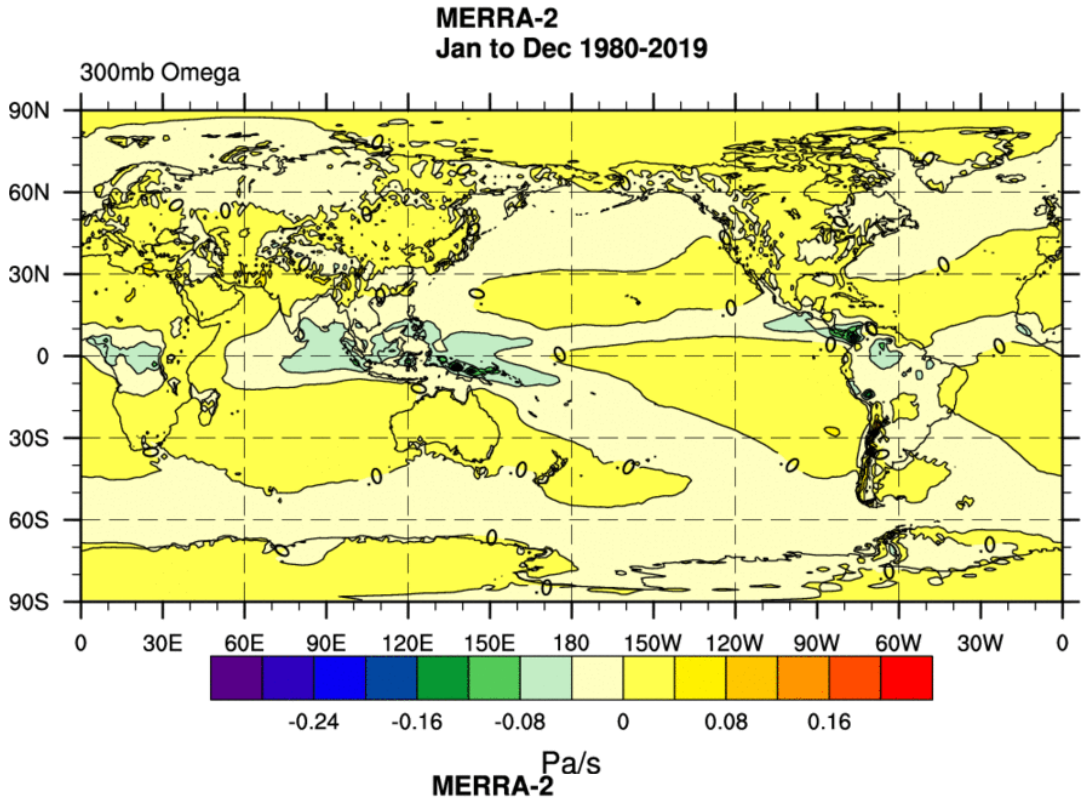

1093

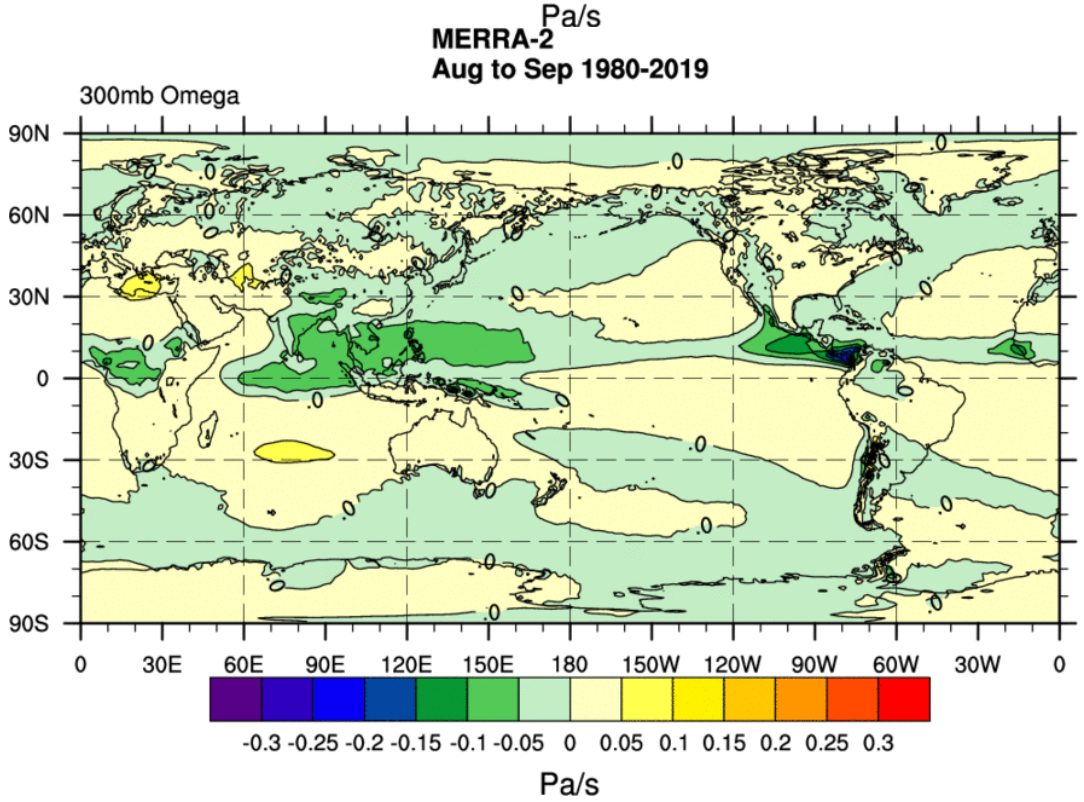

1094

1095 Figure A-3 Annual (top panel) and August-September climatology of 300 hPa Omega (Pa s^{-1}) based on the

1096 Modern-Era Retrospective analysis for Research and Applications, Version 2 (MERRA2) reanalysis.